Journal of Medicinal Chemistry

Article

Discovery of Imidazo[1,2-b]pyridazine Derivatives: Selective and Orally Available Mps1 (TTK) Kinase Inhibitors Exhibiting Remarkable Antiproliferative Activity

Ken-ichi Kusakabe, Nobuyuki Ide, Yataro Daigo, Takeshi Itoh, Takahiko Yamamoto, Hiroshi Hashizume, Kohei Nozu, Hiroshi Yoshida, Genta Tadano, Sachie Tagashira, Kenichi Higashino, Yousuke Okano, Yuji Sato, Makiko Inoue, Motofumi Iguchi, Takayuki Kanazawa, Yukichi Ishioka, Keiji Dohi, Yasuto Kido, Shingo Sakamoto, Shigeru Ando, Masahiro Maeda, Masayo Higaki, Yoshiyasu Baba, and Yusuke Nakamura

J. Med. Chem., **Just Accepted Manuscript** • Publication Date (Web): 27 Jan 2015

Developmental Research Laboratories
Ando, Shigeru; Shionogi Pharmaceutical Research Center, Medicinal Research Laboratories
Maeda, Masahiro; Shionogi Pharmaceutical Research Center, Innovative Drug Discovery Research Laboratories
Higaki, Masayo; Shionogi Pharmaceutical Research Center, Innovative Drug Discovery Research Laboratories
Baba, Yoshiyasu; Shionogi Pharmaceutical Research Center, Medicinal Research Laboratories
Nakamura, Yusuke; The University of Tokyo, Institute of Medical Science

Discovery of Imidazo[1,2-*b*]pyridazine Derivatives: Selective and Orally Available Mps1 (TTK) Kinase Inhibitors Exhibiting Remarkable Antiproliferative Activity

Ken-ichi Kusakabe,[*,†] *Nobuyuki Ide,*[†] *Yataro Daigo,*[#,‡] *Takeshi Itoh,*[†] *Takahiko Yamamoto,*[‖] *Hiroshi Hashizume,*[†] *Kohei Nozu,*[†] *Hiroshi Yoshida,*[†] *Genta Tadano,*[†] *Sachie Tagashira,*[†] *Kenichi Higashino,*[‖] *Yousuke Okano,*[‖] *Yuji Sato,*[†] *Makiko Inoue,*[†] *Motofumi Iguchi,*[†] *Takayuki Kanazawa,*[†] *Yukichi Ishioka,*[†] *Keiji Dohi,*[†] *Yasuto Kido,*[§] *Shingo Sakamoto,*[§] *Shigeru Ando,*[†] *Masahiro Maeda,*[‖] *Masayo Higaki,*[‖] *Yoshiyasu Baba,*[†] *and Yusuke Nakamura*[‡,∞]

[†]Medicinal Research Laboratories, [§]Drug Developmental Research Laboratories, and [‖]Innovative Drug Discovery Research Laboratories, Shionogi Pharmaceutical Research Center, 1-1 Futaba-cho 3-chome, Toyonaka, Osaka 561-0825, Japan.

[‡]Laboratory of Molecular Medicine, Human Genome Center, Institute of Medical Science, The University of Tokyo, 4-6-1 Shirokanedai, Minato-ku, Tokyo 108-8639, Japan.

[#]Department of Medical Oncology, Shiga University of Medical Science, Seta Tsukinowa-cho, Otsu, Shiga 520-2192, Japan.

KEYWORDS: monopolar spindle 1, Mps1, TTK, kinase, inhibitor, imidazo[1,2-*b*]pyridazine, X-ray structure, cellular activity, antiproliferative activity, cancer

ABSTRACT.

Monopolar spindle 1 (Mps1) is an attractive oncology target due to its high expression level in cancer cells as well as the correlation of its expression levels with histological grades of cancers. An imidazo[1,2-*a*]pyrazine **10a** was identified during an HTS campaign. Although **10a** exhibited good biochemical activity, its moderate cellular as well as antiproliferative activities needed to be improved. The cocrystal structure of an analogue of **10a** guided our lead optimization to introduce substituents at the 6-position of the scaffold, giving the 6-aryl substituted **21b** which had improved cellular activity but no oral bioavailability in rat. Property-based optimization at the 6-position and a scaffold change led to the discovery of the imidazo[1,2-*b*]pyridazine-based **27f**, an extremely potent (cellular Mps1 IC_{50} = 0.70 nM, A549 IC_{50} = 6.0 nM) selective Mps1 inhibitor over 192 kinases, which could be orally administered and was active *in vivo*. This **27f** demonstrated remarkable antiproliferative activity in the nanomolar range against various tissue cancer cell lines.

INTRODUCTION

Genetic instability is a hallmark of cancer cells.[1–3] This instability is caused by aneuploidy, with aberrant genomic structures and abnormal numbers of chromosomes. This state is closely linked to chromosomal instability (CIN).[4] While aneuploidy and CIN are considered to be characteristics of cancer cells, normal cells show high intolerance of aneuploidy and CIN. One possible explanation for this is that cancer cells acquire the ability to tolerate aneuploidy or CIN.[5]

Therefore, elucidating the mechanism of how they acquire this ability could offer hints for developing therapeutic strategies for cancer treatment.

Monopolar spindle 1 (Mps1), also known as TTK, is a dual specificity protein kinase that phosphorylates tyrosine, serine, or threonine residues.[6,7] Mps1 has essential roles in mitosis including centrosome duplication, mitotic checkpoint signaling, and the maintenance of CIN.[8−11] Gabrielson et al. reported four important findings related to Mps1 in breast cancer cells.[5] The first was that Mps1 expression levels were correlated with the histological grades of breast cancers. Second, the reduction of Mps1 levels by siRNA in cancer cells decreased their survival and growth resulting in induction of apoptosis, while there was no significant increase in apoptosis in Mps1-depleted nonmalignant cells. Reduced growth of xenografts in mice was also observed after RNAi-mediated decrease in Mps1. The third finding was that reduced Mps1 levels led to aberrant mitoses in breast cancer cells, while a similar level of Mps1 reduction showed successful mitosis in nonmalignant cells, indicating that high levels of Mps1 would be required for the cancer cells to normally progress through mitosis. The fourth finding was that reduced Mps1 levels due to shRNA led to selective survival of cells with less aneuploidy. It was also reported that increased expression of Mps1 was observed in a wide range of cancer cells.[12−15] Thus, the evidence observed with breast cancer cells could be applied to other types of cancers. Taken together, high levels of Mps1 seem to support tolerance of aneuploidy in cancer cells. In other words, inhibition of Mps1 could lead to selective death of cancer cells with aneuploidy, which would be a promising strategy in the development of cancer therapeutics.

Potent and selective Mps1 inhibitors have been discovered.[16−21,42] For example, Nerviano Medical Sciences and Myrexis (Myriad) have reported on **1** (NMS-P715)[23,24] and **2** (MPI-0479605),[25,26] respectively (Chart 1). Recently, Nerviano disclosed its backup compound of **1** as NMS-P153, which showed improved pharmacokinetic profiles and higher *in vivo* efficacy,

although its structure is unknown.[27] Both inhibitors **1** and **2** have pyrimidine-based scaffolds and were shown to inhibit tumor growth in preclinical cancer models. In our efforts to discover Mps1 inhibitors, we identified diaminopyridine-based compound **3** as a selective inhibitor with *in vivo* activity. Its high selectivity was explained by its binding to a flipped-peptide conformation at the hinge region.[28] Indazole-based **4**, which was designed based on a pan-kinase inhibitor SP600125,[30] was also disclosed.[29] These Mps1 inhibitors were very potent according to biochemical assay, while their cellular Mps1 as well as antiproliferative activities in tumor cells showed their moderate *in vivo* potency. The purpose of our present research is to explore selective and orally available Mps1 inhibitors that are extremely potent in cancer cells as well as cancer xenograft models.

High throughput screening of our kinase-focused libraries identified imidazo[1,2-*a*]pyrazine **10a**[31,32] as a potent Mps1 inhibitor with a biochemical IC_{50} value of 55 nM (Table 1), and this was selected as a starting point for our investigation. In parallel with our research, Bayer group identified **10a** as Mps-BAY2b.[32] Further *in vitro* profiling indicated that **10a** showed moderate activity in cellular Mps1 (cellular Mps1 IC_{50} = 276 nM) but lacked antiproliferative activity in A549 lung cancer cells (A549 IC_{50} = 1112 nM). Therefore, we initiated our medicinal chemistry effort to improve the cellular Mps1 as well as the antiproliferative activity of **10a**. Herein, we detail the drug design campaign that led to the discovery of the imidazo[1,2-*b*]pyridazine-based **27f**,[33] a potent antiproliferative and selective Mps1 inhibitor with *in vivo* activity.

CHEMISTRY

The syntheses of imidazo[1,2-*a*]pyrazines **10a**−**d** are illustrated in Scheme 1. Suzuki coupling reaction of compound **7**[34] followed by saponification provided carboxylic acid **8**, which was then coupled with amines using HATU followed by oxidation to give **9a**−**d**. Finally, replacement of

the methylsulfonyl group with isopropyl amine gave compounds **10a−d**. Amine derivatives **11a−f** were synthesized in a manner similar to **10a** (Scheme 2). We introduced various amines to a reflux condition with **9a** to obtain compounds **11a−f**.

To introduce substituents at the 6-position of the imidazo[1,2-*a*]pyrazine scaffold, the synthetic strategy was modified. Starting with compound **12**, the 6-substituted imidazo[1,2-*a*]pyrazines **15a** and **15b** were prepared as shown in Scheme 3. Introduction of the amino group was accomplished using 4-(aminomethyl)tetrahydropyran followed by the Suzuki coupling reaction to obtain compound **14**, which was again coupled by the Suzuki reaction with the corresponding boronic acids to furnish the final compounds **15a** and **15b**.

The syntheses of imidazo[1,2-*b*]pyridazines **21a** and **21b** are illustrated in Scheme 4. Amino group addition to **16**[35] followed by protection of *tert*-butoxycarbonyl (Boc) group afforded **18**. Subsequent iodination of **18** followed by the Suzuki reaction gave the key intermediate **20**, which was then coupled with the corresponding boronic acids and subsequent deprotection to afford imidazo[1,2-*b*]pyridazines **21a** and **21b**.

The syntheses of 6-alkoxy and 6-amino substituted imidazo[1,2-*b*]pyridazines **24a−e** and **27a−f** are illustrated in Scheme 5 and 6. Compounds **24a−e** were prepared from the Boc-protected intermediate **18**. Sodium alkoxides or phenoxides, prepared using sodium hydride, were reacted with **18** to afford **22a−e**, which was iodinated using iodine followed by the Suzuki reaction and deprotection of the Boc group to furnish compounds **24a−e**. The 6-amino substituted **27a-f** were also prepared using intermediate **18** as a starting material (Scheme 6). Compound **18** was subjected to the Buchwald-Hartwig reaction to afford the amines **25a−f**. Conversion of **25a−f** to the target compounds **27a−f** followed the procedures as described in Scheme 5.

RESULTS AND DISCUSSION

SAR of the 3- and 8-Positions: Identification of Lead 11e. We first examined the effect of the amide group at the 3-position of the imidazo[1,2-*a*]pyrazine scaffold in **10a** (Table 1). Even small changes, such as replacement of the cyclopropyl group with either a cyclobutyl (**10b**) or an isopropyl group (**10c**), resulted in a decrease in activity. The primary amide **10d** also led to a 45-fold loss in potency. Along with other data not shown,[33] these results indicated that the cyclopropyl amide group was optimal for Mps1 activity.

To improve the biochemical Mps1 activity of **10a**, a variety of 8-substituted imidazo[1,2-*a*]pyrazines were evaluated (Table 2). Branching at the α-position to the nitrogen such as the isopropyl group (**11b**) diminished the activity, while a linear chain such as the *n*-propyl group was better tolerated (**11a**). Simple changes to the cyclopropylmethyl group (**11d**) improved Mps1 potency, indicating that β-branched chains would be important for binding Mps1. Indeed, the thienylmethyl analogue **11f** retained activity relative to **10a**, although the benzyl analogue (**11c**) resulted in a 2-fold loss in potency. Finally, further exploration of β-branched analogues identified a promising tetrahydro-2*H*-pyranylmethyl analogue **11e** with an IC_{50} value of 35 nM. Importantly, **11e** exhibited improved liver microsomal stability in rat after 30 minutes of incubation (RLM = 71% remaining) when compared with isobutyl **10a**, cyclopropyl **11d**, and thienyl **11f** (RLM = 55%, 35%, and 1% remaining, respectively). With good overall properties, the tetrahydro-2*H*-pyranylmethyl was chosen for further exploration.

Structure-Based Design Using Crystal Structure of Imidazo[1,2-*a*]pyrazine 11f. To enable the design of more potent Mps1 inhibitors, we obtained the cocrystal structure of lead analogue **11f** (Figure 1). The binding mode for **11f** agrees well with the SAR described above at the 3- and 8-positions on the imidazo[1,2-*a*]pyrazine scaffold. For example, the cyclopropyl amide group forms suitable van der Waals interactions in the back pocket, also known as the specificity pocket, explaining why even a slight change such as cyclobutyl **10b** and isopropyl **10c** could not

be tolerated at this position (Figure 1A). Additionally, the poor potency of the α-branched isopropyl **11b** can be explained by disruption of the interaction with the hinge region of the enzyme (Asn606). Finally, the cocrystal structure of **11f** with Mps1 suggested that vectors from the 6-position of the imidazo[1,2-*a*]pyrazine would offer the ability to project toward the ribose binding pocket (Figure 1A). Thus, we hypothesized that introduction of substituents at this position should provide an opportunity to increase the inhibitory activity of Mps1. As this pocket is defined by hydrophobic residues such as Ile663 and Pro673, more hydrophobic substituents would lead to stronger interactions with this pocket.

Initial SAR at the 6-Position of 11e. With the structure-based design described above in mind, we explored substituents at the 6-position on the imidazo[1,2-*a*]pyrazine in **11e**. In addition to improving the biochemical activity of Mps1, the initial goal of our SAR was to identify compounds that were potent in both the cellular Mps1 assay as well as the A549 antiproliferative assay. To evaluate the cellular inhibition of Mps1, we used an autophosphorylation assay on a cell line that stably expresses FLAG-tagged Mps1 under the control of a tetracycline-suppressible promoter.[28] The antiproliferative activity was measured in the A549 lung carcinoma cell line.[28] According to the above design, this region was accessed with a focus on hydrophobic substituents (Table 3). Introduction of the phenyl ring at the 6-position (**15a**) led to a 4-fold increase in biochemical Mps1 IC_{50}. Importantly, a significant increase in both cellular Mps1 and A549 antiproliferative activity was observed in **15a** compared with lead **11e**. Further gains in cellular potency could be found when a cyano group was introduced at the *p*-position on the phenyl ring (**15b**). These results supported the hypothesis that substituents at the 6-position occupy the ribose binding pocket and contribute to an increase in activity. Considering the hinge binding mode of **11f** with Mps1 (Figure 1B), the nitrogen at the 1-position and the amino group at the 8-position on imidazo[1,2-*a*]pyrazine could be expected to be detrimental to the ability to

bind to the hinge. Therefore, we thought that changing scaffolds retaining these atoms such as imidazo[1,2-*b*]pyridazine would maintain the inhibitory activity for Mps1. As expected, changes from the imidazo[1,2-*a*]pyrazine to the imidazo[1,2-*b*]pyridazine (**21a**) retained both biochemical and cellular Mps1 activity relative to the corresponding imidazo[1,2-*a*]pyrazine **15b**. Interestingly, the imidazo[1,2-*b*]pyridazine **21a** showed improved antiproliferative activity (A549 IC_{50} = 39 nM) when compared with **15b**. Further screening of substituents around **21a** revealed that incorporation of an amino group at the *o*-position on the phenyl ring (**21b**) led to increase in activity and exhibited a more favorable cell-shift.

The pharmacokinetic (PK) properties of **15b**, **21a**, and **21b** were characterized in male Sprague-Dawley (SD) rats after intravenous (iv) and oral dosing (Table 6). The imidazo[1,2-*b*]pyridazine **21a** showed lower iv clearance than **15a** due to its improved microsomal stability but exhibited no oral bioavailability in rat. Although the compounds with phenyl groups at the 6-position such as **15b**, **21a**, and **21b** satisfied the initial goal of identifying compounds in cellular assay, these compounds displayed poor pharmacokinetic profiles in rat. Further characterization revealed that these compounds had poor solubility in buffer containing sodium taurocholate at pH 6.8. Indeed, compounds **15b**, **21a**, and **21b** exhibited thermodynamic solubilities of 1.0 μg/mL, 0.49 μg/mL, and 2.6 μg/mL, respectively, while the rat liver microsomal (RLM) stability of 6-substituted **21a** and **21b** showed acceptable values (42% and 59% remaining after 30 min incubation, respectively) resulting in low to moderate clearance in rat (38 and 23 ml/min/kg, respectively). In contrast, non-substituted **15b** exhibited high clearance (145 ml/min/kg) associated with low metabolic stability (0% remaining), suggesting that increasing the solubility of 6-substituted **21a** and **21b** might improve the bioavailability.

Optimization at the 6-Position to Obtain 27f. To improve the oral bioavailability of the 6-substituted imidazo[1,2-*b*]pyridazines such as **21a** and **21b** by increasing solubility, we focused

on inserting hetroatoms at the 6-position. Given that this position occupies the lipophilic ribose binding pocket, designing substituents with a favorable lipophilicity would be important for striking a balance between cellular activity and oral bioavailability. As shown in Table 4, we first examined alkoxy analogues with the imidazo[1,2-*b*]pyridazine scaffold. Phenoxy **24b** was equipotent with *p*-cyanophenyl **21a**, while cyclohexyloxy **24a** resulted in a decrease in cellular activity. Addition of the *p*-fluoro (**24c**) imparted a 2-fold decrease in both cellular Mps1 and A549 antiproliferative activities; *o*-fluoro **24d** retained cellular potency relative to non-substituted **24b**. Interestingly, incorporation of the o-hydroxyl group (**24e**) gave excellent cellular Mps1 potency along with the highest antiproliferative activity in A549 cells with an IC_{50} value of 2.0 nM.

The selected alkoxy analogues **24a**, **24d**, and **24e** were assessed for the rat PK profile following the thermodynamic solubility and RLM stability (Table 6). As expected, **24a** and **24d** displayed improved solubility and also retained metabolic stability, which translated into improved rat oral bioavailability (23% and 16%, respectively). However, **24e** with the highest potency had poor solubility and low metabolic stability regardless of its lower lipophilicity relative to **24a** and **24d** (cLogP[36]: **24a**: 4.8; **24d**: 4.6; **24e**: 3.7), resulting in no oral bioavailability and high clearance in rat. Taken together, incorporation of an oxygen atom at the 6-position led to improved cellular potency and oral bioavailability, which provided a good opportunity to further optimize potency and PK profiles by using other heteroatoms.

Next, we turned our attention to inserting a nitrogen atom at the 6-position (Table 5). Unlike the SAR observed with alkoxy analogues **24a** and **24b**, cyclohexylamino **27b** was more potent than phenylamino **27a**. Cyclopentyl **27c** was equipotent to cyclohexyl **27b**. Truncating the cyclohexyl group by an isopropyl (**27d**) resulted in retained biochemical activity but reduced cellular activity. Interestingly, bulky *tert*-butylamino **27e** showed improvement of both cellular

Mps1 and A549 antiproliferative activities when compared with isopropyl **27d**. Screening a series of bulky alkylamino groups led to the identification of compound **27f** bearing a CF_3 group, which exhibited excellent cellular potency (cellular Mps1 IC_{50} = 0.70 nM, A549 IC_{50} = 6.0 nM).

The aqueous solubility of the amino analogue **27f** was better than that of aryl and alkoxy analogues, while the *in vitro* metabolic stability was comparable to these compounds (Table 6). Consistent with its improved solubility, compound **27f** showed favorable oral exposure at a dose of 1 mg/kg (C_{max} = 38 ng/ml, F = 24%). A similar tendency was confirmed with *tert*-butylamino **27e** that had acceptable solubility of 63 μg/ml, which was translated into oral bioavailability (F = 36%).

Crystal Structure of Imidazo[1,2-*b*]pyridazine 27b Bound to Mps1. To determine the binding mode of imidazo[1,2-*b*]pyridazines with substituents at the 6-position and to test our design hypothesis, the crystal structure of **27b**, an analogue of **27f**, bound to Mps1 was obtained (Figure 2). The binding mode of **27b** is nearly consistent with that in **11f** (overlay of **11f** and **27b** bound to Mps1 is shown in Supporting Information, Figure S1) As expected, the cyclohexylamino group at the 6-position occupies the sugar pocket (Figure 2A and B). Like **11f**, the cyclopropyl amide group forms suitable van der Waals interactions in the back pocket (Figure 2A) and also has hydrogen bond interactions with the amine NH_3^+ of Lsy553 and the amide carbonyl of Ile663 (Figure 2C and D). The imidazo[1,2-*b*]pyridazine scaffold in **27b** maintains the key hydrogen bond donor-acceptor interaction with the hinge region of Mps1 like the imidazo[1,2-*a*]pyrazine in **11f** (Figure 2C). Consistent with other Mps1 crystal structures, this was found to adopt an active kinase conformation because we observed the presence of the Lys553-Glu571 salt bridge and the DFG-in conformation. An important feature of the crystal structure of Mps1 is an antiparallel β-sheet between the activation loop and the phosphate-binding loop (P-loop): Ser553 in the activation loop forms a hydrogen bond donor-acceptor

interaction with Gln672 in the P-loop, which provides the more defined sugar pocket (Figure 2B). Similar findings were observed for the crystal structures of Mps1 with Mps1-IN-2,[18] CCT251455,[21] **3**,[28] and **4**.[29]

Correlation between Cellular Mps1 and A549 Antiproliferative Activity. As described in our previous reports, Mps1 inhibitors with diaminopyridine and indazole scaffolds including **3** and **4** showed excellent correlation between cellular Mps1 and A549 antiproliferative activity.[28,29] To confirm this, we analyzed the relationship using the compounds described in Tables 1−5 (Figure 3). The potent compounds in the cellular assays (**21b**, **24e**, and **27f**) are highlighted in green. Figure 3A shows a correlative plot of biochemical and cellular Mps1 IC_{50} values (R^2 = 0.917), which implies that these compounds had acceptable permeability to possess cellular activity. Consistent with our previous Mps1 inhibitors, we observed an excellent correlation between cellular Mps1 and A549 IC_{50} values (Figure 3B; R^2 = 0.969), indicating that improved antiproliferative activity particularly observed with **21b**, **24e**, and **27f** could be considered responsible for the increased activity of Mps1.

Kinase Selectivity Profiles of 11e, 24e, and 27f. Understanding the off-target kinase inhibition is crucial to help interpret the cellular signaling. The cellular active compounds **24e** and **27f** were profiled against a panel of 192 kinases at concentrations of 0.2 μM and 1 μM (Supporting Information, Table S1). For comparison, **11e**, which has no substituent at the 6-position, was also profiled against a smaller panel of 122 kinases at a concentration of 1 μM. Compound **27f** displayed excellent selectivity over 192 kinases. Although only two kinases (CAMK1 and CLK2) were inhibited by more than 50% by **27f** at 1 μM, no significant inhibition over 192 kinases (>50%) was observed at 0.2 μM. Compound **24e** also inhibited two kinases (ABL_G250E and CLK2) out of 192. Unlike **27f**, CLK2 was inhibited by more than 50% even at 0.2 μM, while ABL_G250E was not.

To gain insight into the effects of the substituents at the 6-position that occupy the ribose binding pocket, non-substituted **11e** was profiled over a panel of 122 kinases. Although this panel did not include CAMK1 and CLK2 (but did include ABL_G250E), **11e** showed no significant inhibition (>50%) over the kinases, indicating that the substituents at the 6-position in the ribose binding pocket would not affect the kinase selectivity. This result was consistent with our previous results observed with indazole derivatives such as **4**; the size of substituents in the ribose binding pocket did not affect the selectivity, while those in the back pocket were important for gaining selectivity.[29] According to the X-ray structures of **11b** and **27b**, the cyclopropyl amide in compounds **11e**, **24e**, and **27f** have excellent van der Waals contacts with the back pocket. Indeed, slight structural changes such as cyclobutyl **10b** and isopropyl **10c** were not tolerated in this region. Therefore, we hypothesized that the high selectivity of these compounds may arise from the interaction of the cyclopropyl amide with the back pocket.

Antiproliferative Activity of 27f against Various Cancer Cell Lines. To ascertain the effect of Mps1 inhibition on tumor growth derived from various tissues, the antiproliferative effects of compound **27f** against a panel of 13 tumor cell lines and a non-transformed cell line MRC-5 were examined as shown in Table 7. For comparison, the antiproliferative activities of paclitaxel (**28**)[37] and MLN-8237 (**29**),[38] an Aurora A kinase inhibitor, are given in the same Table. After 72 h of treatment, compound **27f** suppressed tumor cell proliferation with IC_{50} values ranging from 3.3 to 320 nM regardless of tumor cell types, which was comparable to **28** and more active than **29**. Importantly, a non-transformed cell line MRC-5 was less sensitive to **27f** with an IC_{50} value of >10 μM, while treatment of **28** in MRC-5 elicited an antiproliferative effect with an IC_{50} value of 80 nM. Like **27f**, no significant decrease in cell viability was observed when treated with Aurora kinase inhibitor **29** in MRC-5.

Tumor Xenograft Study of 27f. On the basis of this promising profile, **27f** was further characterized though a PK study conducted with a preclinical species of nu/nu mice. Consistent with the rat PK profile, good oral exposure in the mice was observed when dosed at 10 and 100 mg/kg (Table 8). To determine the unbound drug level, the plasma protein binding of **27f** was determined. As a result, the free plasma concentration of **27f** at 10 mg/kg was found to be 24 nM (f_u = 0.51%), which was sufficient to induce an *in vivo* effect considering the antiproliferative IC_{50} values. Multiple doses of **27f** were administered daily for 2 weeks to nude mice bearing NCI-H460 lung cancer xenografts (n = 6). Based on the above data, the doses chosen were 2.5, 5, and 10 mg/kg. When dosed at 5 and 10 mg/kg, significant body weight loss and death were observed (Supporting Information, Figure S2; body weight loss of 25 and 32% relative to vehicle-treated mice, one and three deaths, respectively). The lowest dose of 2.5 mg/kg induced tumor growth inhibition (tumor growth inhibition factor T/C = 57%) without significant body weight loss, and doses of 5 and 10 mg/kg also exhibited T/C values of 40% and 19%, respectively, associated with toxicity as shown in Figure 4.

Recently, Mps1 inhibitors **1**[23] and **3**[28] were shown to have significant antitumor activity with no significant body weight loss. In contrast, administration of compound **2** to mice led to tumor growth inhibition associated with significant toxicity (body weight loss and death).[25] As for *in vitro* studies, when Mp1-INI-1 was treated with HCT116 and normal colorectal cells, both cell lines showed loss of viability,[18] while there was no significant effect in nonmalignant MCF10A cells after reduction of Mps1 levels by siRNA.[5] Thus, contradictory results were reported when inhibiting the Mps1 function in both *in vitro* and *in vivo* studies. Although the cause of the toxicity observed with **27f** is unclear, combination therapy, such as with tubulin-targeting agents, may provide an opportunity to not only reduce toxicity but also enhance efficacy as discussed in other reports.[25,32(c),41] The imidazo[1,2-*b*]pyridazine derivatives disclosed in this report such as

27f showed one of the highest cellular Mps1 and antiproliferative activities of known Mps1 inhibitors. More importantly, a clear correlation between cellular Mps1 and antiproliferative IC_{50} was seen in our series, and **27f** was selective over 192 kinases, indicating that the antiproliferative activity may derive from Mps1 inhibition as shown in above. Therefore, these selective Mps1 inhibitors, particularly **27f**, can serve as important probes for investigating the biological role and the cancer therapeutic potential of Mps1.

CONCLUSIONS

We identified the selective Mps1 inhibitor **27f** with remarkable antiproliferative activity, starting from an HTS hit **10a** with an imidazo[1,2-*a*]pyrazine scaffold. Introduction of substituents at the 6-positon and the change to an imidazo[1,2-*b*]pyridazine scaffold led to significant improvement of biochemical and cellular activities, as found with compound **21b**. Further property-based design around **21b** led to the discovery of imidazo[1,2-*b*]pyridazine derivatives with good oral bioavailability and excellent cellular activity. We observed a strong correlation between cellular Mps1 and A549 IC_{50} values, and representative compounds such as **11e**, **24f**, and **27f** demonstrated excellent kinase selectivity, indicating that the improved antiproliferative activity observed in our series would be responsible for the increased activity of Mps1. The *in vivo* result of **27f** showed significant tumor growth inhibition associated with toxicity. Further investigation on dose regimens and combination drugs such as tubulin-targeting agents may improve the therapeutic potentials of **27f**. Finally, we believe that compound **27f** can contribute to further clarifying the biological roles of Mps1 due to its excellent cellular activity and kinase selectivity.

EXPERIMENTAL SECTION

General Chemistry. All commercial reagents and solvents were used as received unless otherwise noted. Thin layer chromatography (TLC) analysis was performed using Merck silica gel 60 F_{254} thin layer plates (250 µm in thickness). Flash column chromatography was carried out on an automated purification system using Yamazen prepacked silica gel columns. ^{1}H NMR spectra were recorded on a Varian Gemini 300 MHz. Spectral data are reported as follows: chemical shift (as ppm referenced to tetramethylsilane), multiplicity (s = singlet, d = doublet, dd = double doublets, dt = double triplet, t = triplet, q = quartet, m = multiplet, br = broad peak), coupling constant, and integration value. Analytical LC/MS was performed on a Waters X-Bridge (C18, 5 µm, 4.6 mm × 50 mm, a linear gradient from 10% to 100% B over 3 min and then 100% B for 1 min (A = H_2O + 0.1% formic acid, B = MeCN + 0.1% formic acid), flow rate 3.0 mL/min) using a Waters system equipped with a ZQ2000 mass spectrometer, 2525 binary gradient module, 2996 photodiode array detector (detection at 254 nm), and 2777 sample manager. Preparative LC/MS was performed on a Waters X-Bridge (C18, 5 µm, 19 mm × 50 mm, a linear gradient from 10% to 100% B over 5 min and then 100% B for 2 min (A = H_2O + 0.1% formic acid, B = MeCN + 0.1% formic acid), flow rate 25 mL/min) using a Waters system equipped with a ZQ2000 mass spectrometer, 2525 binary gradient module, 2996 photodiode array detector (detection at 254 nm), and 2777 sample manager. The purity of all compounds used in the bioassays was determined by this method to be >95%. High resolution mass spectra were recorded on a Thermo Fisher Scientific LTQ Orbitrap using electrospray positive ionization.

4-(8-(Methylthio)imidazo[1,2-*a*]pyrazin-3-yl)benzoic acid (8). A mixture of **7** (3.00 g, 12.3 mmol), 4-methoxycarbonylphenylboronic acid pinacol ester (4.19 g, 16.0 mmol), $PdCl_2$(dppf)·DCM (1.00 g. 1.23 mmol), and Na_2CO_3 (2 M solution in water, 12.3 mL, 24.6 mmol) in dioxane (60 mL) was heated to reflux for 3 h under a nitrogen atmosphere. The

reaction mixture was allowed to cool to room temperature and diluted with water and EtOAc. The aqueous layer was separated and extracted with EtOAc. The combined organic extracts were washed with water and brine, dried over $MgSO_4$, filtered, and concentrated. The residue was purified by flash chromatography (silica gel; EtOAc/hexane, gradient: 20−60% EtOAc) to afford methyl 4-(8-(methylthio)imidazo[1,2-*a*]pyrazin-3-yl)benzoate (3.03 g, 82%) as a white solid. ^{1}H NMR (400 MHz, DMSO-d_6) δ 2.62 (s, 3H), 3.90 (s, 3H), 7.85 (d, J = 4.5 Hz, 1H), 7.88 (d, J = 8.0 Hz, 2H), 8.03 (s, 1H), 8.11 (d, J = 8.0 Hz, 2H), 8.41 (d, J = 4.5 Hz, 1H). MS-ESI (*m/z*) = 300 $[M+H]^+$. To a solution of this compound (309 mg, 1.03 mmol) in THF/methanol (1:1, 18 mL) was added aqueous LiOH solution (4 M; 516 µL, 2.06 mmol) at room temperature. The reaction mixture was stirred overnight and then acidified with aqueous HCl solution (2 M; 1.1 mL). The organic solvents were evaporated, and the resulting mixture was diluted with EtOAc. The aqueous layer was separated and extracted with EtOAc. The combined organic extracts were washed with water and brine, dried over $MgSO_4$, filtered, and concentrated to afford **8** (301 mg, quant.) as an off-white solid. ^{1}H NMR (400 MHz, DMSO-d_6) δ 2.62 (s, 3H), 7.82−7.89 (m, 4H), 8.02 (s, 1H), 8.10 (d, J = 8.0 Hz, 2H), 8.41 (d, J = 4.8 Hz, 1H), 13.16 (br. s., 1H). MS-ESI (*m/z*) = 286 $[M+H]^+$.

***N*-Cyclopropyl-4-(8-(methylsulfonyl)imidazo[1,2-*a*]pyrazin-3-yl)benzamide (9a).** To a solution of **8** (100 mg, 0.350 mmol), DIEA (122 µL, 0.701 mmol), and HATU (160 mg, 0.421 mmol) in DCM (2 mL) was added cyclopropylamine (30 µL, 0.421 mmol) at room temperature. The reaction mixture was stirred for 4 h and then diluted with water and DCM. The aqueous layer was separated and extracted with DCM. The combined organic extracts were dried over $MgSO_4$, filtered, and concentrated to afford *N*-cyclopropyl-4-(8-(methylthio)imidazo[1,2-*a*]pyrazin-3-yl)benzamide (127 mg) as a pale yellow solid. ^{1}H NMR (400 MHz, DMSO-d_6) δ 0.57−0.63 (m, 2H), 0.72 (s, 2 H), 2.59−2.65 (m, 3H), 2.84−2.94 (m, 1H), 7.80 (d, J = 8.0 Hz, 2H),

7.84 (d, J = 4.5 Hz, 1H), 7.96−8.04 (m, 3H), 8.37 (d, J = 4.5 Hz, 1H), 8.57 (d, J = 3.8 Hz, 1H). MS-ESI (*m/z*) = 325 $[M+H]^+$. A mixture of this compound (121 mg, 0.373 mmol) and *m*-CPBA (69% wt, 280 mg, 1.12 mmol) in DCM (3 mL) was stirred at room temperature for 3 h. The reaction mixture was diluted with water and DCM. The aqueous layer was separated and extracted with DCM. The combined organic extracts were washed with saturated aqueous $NaHCO_3$ solution and brine, dried over $MgSO_4$, and concentrated. The residue was purified by flash chromatography (silica gel; EtOAc/hexane, gradient: 50−100% EtOAc) to afford **9a** (110 mg, 88%) as a yellow amorphous substance. ^{1}H NMR (400 MHz, $CDCl_3$) δ 0.65−0.71 (br m, 2H), 0.89−0.96 (m, 2H), 2.92−3.00 (br m, 1H), 3.58 (s, 3H), 7.64 (d, J = 7.5 Hz, 2H), 7.96 (d, J = 7.5 Hz, 2H), 8.06 (d, J = 4.4 Hz, 1H), 8.10 (s, 1H), 8.43 (d, J = 4.4 Hz, 1H). MS-ESI (*m/z*) = 357 $[M+H]^+$.

***N*-Cyclopropyl-4-(8-(isobutylamino)imidazo[1,2-*a*]pyrazin-3-yl)benzamide (10a)**. A mixture of **9a** (62.7 mg, 0.176 mmol) and isobutylamine (87 µL, 0.88 mmol) in dioxane (1.0 mL) was heated to reflux for 12 h. The reaction mixture was allowed to cool to room temperature and diluted with water and EtOAc. The aqueous layer was separated and extracted with EtOAc The combined organic extracts were washed with water and brine, dried over $MgSO_4$, and concentrated. The residue was purified by flash chromatography (silica gel; EtOAc/hexane, gradient, 50−90% EtOAc) to afford **10a** (58.3 mg, 95%) as a yellow solid. ^{1}H NMR (400 MHz, DMSO-d_6) δ 0.58−0.62 (m, 2H), 0.70−0.74 (m, 2H), 0.91 (d, J = 6.8 Hz, 6H), 2.00−2.07 (m, 1H), 2.85−2.92 (m, 1H), 3.29−3.35 (m, 2H), 7.35 (d, J = 4.8 Hz, 1H), 7.57 (t, J = 5.8 Hz, 1H), 7.74−7.76 (m, 3H), 7.80 (s, 1H), 7.98 (d, J = 8.0 Hz, 2H), 8.54 (d, J = 3.8 Hz, 1H). HRMS-ESI (*m/z*): $[M+H]^+$ calcd for $C_{20}H_{24}N_5O$, 350.1975; found, 350.1975.

6-Bromo-3-iodo-*N*-((tetrahydro-2*H*-pyran-4-yl)methyl)imidazo[1,2-*a*]pyrazin-8-amine (13). A solution of **12** (1.58 g, 3.92 mmol) and 4-(aminomethyl)tetrahydropyran (1.34 g, 11.8

mmol) in DMA (7.9 mL) was heated in microwave reactor at 130 °C for 20 min. The reaction mixture was diluted with water, and the resulting solid was collected on a glass filter to afford **13** (1.66 g, 97%) as a white solid. ^{1}H NMR (300 MHz, DMSO-d_6) δ 1.21 (ddd, J = 24.2, 11.9, 3.8 Hz, 2H), 1.59 (d, J = 12.5 Hz, 2H), 1.89−2.00 (br m, 1H), 3.25 (t, J = 11.4 Hz, 2H), 3.83 (d, J = 10.5 Hz, 2H), 7.60 (s, 1H), 7.64 (s, 1H), 8.15 (t, J = 5.6 Hz, 1H). MS-ESI (m/z) = 436.9 $[M+H]^+$.

4-(6-Bromo-8-((tetrahydro-2*H*-pyran-4-yl)methylamino)imidazo[1,2-*a*]pyrazin-3-yl)-*N*-cyclopropylbenzamide (14). A mixture of **13** (1.66 g, 3.80 mmol), $Pd(PPh_3)_4$ (220 mg, 0.190 mmol), Na_2CO_3 (2 M in water, 3.8 mL), and 4-(cyclopropylaminocarbonyl)phenylboronic acid pinacol ester (1.09 g, 3.80 mmol) was heated in microwave reactor at 130 °C for 20 min. The reaction mixture was diluted with $CHCl_3$ and water, and then filtered through celite. The aqueous layer was separated and extracted with $CHCl_3$. The combined extracts were washed with water and brine, dried over $MgSO_4$, filtered, and concentrated. The resulting solid was collected on a glass filter to afford **14** (1.47 g, 82%) as a tan solid. ^{1}H NMR (400 MHz, DMSO-d_6) δ 0.58−0.62 (m, 2H), 0.72 (q, J = 6.1 Hz, 2H), 1.24 (ddd, J = 24.4, 12.0, 3.8 Hz, 2H), 1.61 (d, J = 12.3 Hz, 2H), 1.91−2.02 (br m, 1H), 2.85−2.91 (m, 1H), 3.27 (t, J = 11.4 Hz, 2H), 3.85 (d, J = 9.8 Hz, 2H), 7.74 (d, J = 8.0 Hz, 2H), 7.80 (br s, 2H), 7.98 (d, J = 8.0 Hz, 2H), 8.16 (t, J = 5.6 Hz, 1H), 8.54 (d, J = 3.8 Hz, 1H). MS-ESI (m/z) = 470 $[M+H]^+$.

4-(6-(4-Cyanophenyl)-8-((tetrahydro-2*H*-pyran-4-yl)methylamino)imidazo[1,2-*a*]pyrazin-3-yl)-*N*-cyclopropylbenzamide (15b). A mixture of **14** (188 mg, 0.400 mmol), 4-cyanophenylboronic acid (58.7 mg, 0.400 mmol), Na_2CO_3 (2 M in water, 0.40 mL), and $PdCl_2(PPh_3)_4$ (14.0 mg, 0.0200 mmol) was heated in microwave reactor at 130 °C for 10 min. The reaction mixture was diluted with $CHCl_3$ and water, and then filtered through celite. The aqueous layer was separated and extracted with $CHCl_3$. The combined extracts were washed with water and brine, dried over $MgSO_4$, filtered, and concentrated. The mixture was purified by

preparative LC/MS to afford **15b** (107 mg, 54%) as a tan solid. ^{1}H NMR (400 MHz, DMSO-d_6) δ 0.58−0.62 (m, 2H), 0.72 (q, J = 6.1 Hz, 2H), 1.30 (ddd, J = 24.3, 12.0, 3.7 Hz, 2H), 1.66 (d, J = 12.8 Hz, 2H), 1.98−2.09 (br m, 1H), 2.86−2.93 (m, 1H), 3.27 (t, J = 11.5 Hz, 2H), 3.53 (t, J = 6.3 Hz, 2H), 3.86 (d, J = 9.8 Hz, 2H), 7.82−7.84 (m, 3H), 7.88−7.91 (m, 3H), 8.01 (d, J = 7.8 Hz, 2H), 8.22 (d, J = 8.0 Hz, 2H), 8.30 (s, 1H), 8.56 (d, J = 4.0 Hz, 1H). MS-ESI (*m/z*) = 493 $[M+H]^+$. HRMS-ESI (*m/z*): [M+H]+ calcd for $C_{29}H_{29}N_6O_2$, 493.2347; found, 493.2349.

6-Chloro-*N*-((tetrahydro-2*H*-pyran-4-yl)methyl)imidazo[1,2-*b*]pyridazin-8-amine (17). A mixture of **16** (4.85 g, 15.9 mmol), 4-aminomethyltetrahydropyran (3.11 g, 27 mmol), and DIEA (8.32 mL, 47.6 mmol) in ethanol (40 mL) was heated to reflux for 15 h. The reaction mixture was allowed to cool to room temperature and then diluted with water and EtOAc. The aqueous layer was separated and extracted with EtOAc. The combined extracts were washed with brine, dried over $MgSO_4$, filtered, and evaporated. The residue was purified by flash column chromatography (silica gel, EtOAc/hexane, gradient: 25−70% EtOAc) to afford **17** (2.99 g, 71%) as a brown solid. ^{1}H NMR (300 MHz, DMSO-d_6) δ 1.21 (ddd, J = 24.8, 11.9, 4.4 Hz, 2H), 1.60 (dd, J = 12.7, 1.9 Hz, 2H), 1.87−1.95 (m, 1H), 3.20−3.28 (m, 4H), 3.82 (dd, J = 11.4, 2.7 Hz, 2H), 6.23 (s, 1H), 7.49 (d, J = 1.2 Hz, 1H), 7.95 (t, J = 5.6 Hz, 1H), 7.97 (d, J = 1.2 Hz, 1H). MS-ESI (*m/z*) = 267 $[M+H]^+$.

***tert*-Butyl 6-chloroimidazo[1,2-*b*]pyridazin-8-yl((tetrahydro-2*H*-pyran-4-yl)methyl)carbamate (18).** A solution of **17** (15.0 g, 56.2 mmol), Boc_2O (26.5 mL, 124 mmol), and DMAP (0.687 g, 5.62 mmol) in THF (150 mL) was heated at 50 °C for 1 h. The reaction mixture was allowed to cool to room temperature and then diluted with EtOAc and water. The aqueous layer was separated and extracted with EtOAc. The combined extracts were washed with brine, dried over $MgSO_4$, filtered, and evaporated. The residue was purified by flash column chromatography (silica gel; EtOAc/hexane, gradient: 10−70% EtOAc) to afford **18** (22.7 g,

110%) as a yellow oil. ^{1}H NMR (300 MHz, DMSO-d_6) δ 1.06−1.20 (m, 2H), 1.35 (s, 9H), 1.54 (d, J = 11.7 Hz, 2H), 1.63−1.72 (m, 1H), 3.15 (t, J = 10.8 Hz, 2H), 3.76 (dd, J = 11.3, 2.9 Hz, 2H), 3.93 (d, J = 7.3 Hz, 2H), 7.46 (s, 1H), 7.81 (t, J = 0.9 Hz, 1H), 8.32 (d, J = 1.1 Hz, 1H). MS-ESI (m/z) = 367 $[M+H]^+$.

***tert*-Butyl 6-chloro-3-iodoimidazo[1,2-*b*]pyridazin-8-yl((tetrahydro-2*H*-pyran-4-yl)methyl)carbamate (19).** A solution of **18** (70.9 g, 193 mmol) and NIS (51.4 g, 228 mmol) in DMF (567 mL) was heated at 80 °C for 9 h. The mixture was allowed to cool to room temperature and diluted with EtOAc and water. The aqueous layer was separated and extracted with EtOAc. The combined extracts were washed with water, aqueous $Na_2S_2O_3$ solution, and brine, dried over $MgSO_4$, filtered, and evaporated. The residue was purified by flash chromatography (silica gel; EtOAc/hexane, 15% EtOAc) to afford **19** (83.9 g, 89%) as a pale yellow solid. ^{1}H NMR (300 MHz, $CDCl_3$) δ 1.28−1.33 (m, 2H), 1.50 (s, 9H), 1.58 (dd, J = 12.8, 1.8 Hz, 2H), 1.74−1.79 (m, 1H), 3.30 (td, J = 11.7, 2.1 Hz, 2H), 3.93 (dd, J = 11.4, 2.5 Hz, 2H), 4.18 (d, J = 7.2 Hz, 2H), 7.19 (s, 1H), 7.80 (s, 1H).

***tert*-Butyl 6-chloro-3-(4-(cyclopropylcarbamoyl)phenyl)imidazo[1,2-*b*]pyridazin-8-yl((tetrahydro-2H-pyran-4-yl)methyl)carbamate (20).** A mixture of **19** (71.0 g, 144 mmol), 4-(cyclopropylaminocarbonyl)phenylboronic acid pinacol ester (49.7 g, 173 mmol), $Pd(PPh_3)_4$ (8.33 g, 7.20 mmol), and Na_2CO_3 (21.4 g, 202 mmol) in DMF/H_2O (426 mL/101 mL) was heated at 100 °C for 7 h. The reaction mixture was allowed to cool to room temperature and diluted with EtOAc and water. The aqueous layer was separated and extracted with EtOAc. The combined extracts were washed with water, dried over $MgSO_4$, filtered, and concentrated. The residue was purified by flash column chromatography (silica gel; EtOAc/hexane, gradient: 40−60% EtOAc) to afford **20** (41.7 g, 55%) as a yellow amorphous substance. ^{1}H NMR (300 MHz, $CDCl_3$) δ 0.63−0.68 (m, 2H), 0.87−0.93 (m, 2H), 1.26−1.37 (m, 2H), 1.50 (s, 9H), 1.59 (d, J = 12.4 Hz,

2H), 1.72−1.83 (m, 1H), 2.90−2.98 (m, 1H), 3.25−3.34 (m, 2H), 3.92 (dd, *J* = 11.7, 2.8 Hz, 2H), 4.18 (d, *J* = 7.2 Hz, 2H), 6.39 (br s, 1H), 7.15 (s, 1H), 7.88 (d, *J* = 8.4 Hz, 2H), 8.04 (s, 1H), 8.12 (d, *J* = 8.4 Hz, 2H).

4-(6-(4-Cyanophenyl)-8-((tetrahydro-2*H*-pyran-4-yl)methylamino)imidazo[1,2-*b*]pyridazin-3-yl)-*N*-cyclopropylbenzamide (21a). A mixture of **20** (245 mg, 0.467 mmol), 4-cyanophenylboronic acid (129 mg, 0.877 mmol), $PdCl_2$(dppf)·DCM (35.8 mg, 0.044 mmol), and Na_2CO_3 (65 mg, 0.614 mmol) in ethanol/H_2O (2.5 mL/0.31 mL) was heated to reflux for 1 h. The reaction mixture was allowed to cool to room temperature and then diluted with EtOAc and water. The aqueous layer was separated and extracted with EtOAc. The combined extracts were washed with water and brine, dried over $MgSO_4$, filtered, and concentrated. The residue was purified by flash column chromatography (silica gel; EtOAc/hexane, gradient: 65−75% EtOAc) to afford *tert*-butyl 6-(4-cyanophenyl)-3-(4-(cyclopropylcarbamoyl)phenyl)imidazo[1,2-*b*]pyridazin-8-yl((tetrahydro-2*H*-pyran-4-yl)methyl)carbamate (277 mg, 107%) as a yellow solid. ^{1}H NMR (300 MHz, $CDCl_3$) δ 0.68 (br s, 2H), 0.84−0.90 (br m, 2H), 1.26−1.39 (m, 2H), 1.54 (s, 9H), 1.63 (d, *J* = 12.6 Hz, 2H), 1.74−1.90 (br m, 1H), 2.89−2.98 (br m, 1H), 3.29 (t, *J* = 11.3 Hz, 2H), 3.92 (d, *J* = 10.1 Hz, 2H), 4.23 (d, *J* = 6.9 Hz, 2H), 6.91 (s, 1H), 7.61 (s, 1H), 7.81 (d, *J* = 8.1 Hz, 2H), 7.94 (d, *J* = 8.1 Hz, 2H), 8.09−8.17 (m, 5H). To this compound in DCM (2.4 mL) was added TFA (2.4 mL) at room temperature. The reaction mixture was stirred for 20 min and then poured into aqueous K_2CO_3 solution. The mixture was diluted with DCM, THF, and water. The aqueous layer was separated and extracted with DCM/THF (2:5). The mixture was washed with brine, dried over Na_2SO_4, filtered, and concentrated. The residue was diluted with EtOAc (8.0 mL) and heated to reflux. After cooling, the resulting solid was collected on a glass filter to afford **21a** (139 mg, 60%) as an off-white solid. ^{1}H NMR (300 MHz, DMSO-d_6) δ 0.56−0.63 (m, 2H), 0.67−0.74 (m, 2H), 1.22−1.36 (m, 2H), 1.66 (d, *J* = 11.9 Hz, 2H), 1.94−2.05 (m, 1H),

2.83−2.91 (m, 1H), 3.22−3.39 (m, 4H), 3.85 (d, *J* = 9.9 Hz, 2H), 6.82 (s, 1H), 7.75−7.80 (m, 1H), 7.95 (d, *J* = 8.4 Hz, 2H), 8.01 (d, *J* = 8.4 Hz, 2H), 8.12 (s, 1H), 8.26−8.31 (m, 4H), 8.48 (d, *J* = 4.1 Hz, 1H). MS-ESI (*m/z*) = 493 $[M+H]^+$.

***tert*-Butyl 6-(cyclohexyloxy)imidazo[1,2-*b*]pyridazin-8-yl((tetrahydro-2*H*-pyran-4-yl)methyl)carbamate (22a).** To a solution of cyclohexanol (259 μL, 2.45 mmol) in NMP (1.5 mL) was added NaH (60% in mineral oil; 82 mg, 2.04 mmol) at room temperature. The mixture was heated to 50 °C for 10 min and then cooled to 0 °C. A solution of **18** (300 mg, 0.818 mmol) in NMP (1.5 mL) was added to this solution, and the reaction mixture was stirred at room temperature for 1.5 h. The mixture was diluted with aqueous citric acid solution and EtOAc. The aqueous layer was separated and extracted with EtOAc. The combined organic layer was washed with water and brine, dired over Na_2SO_4, filtered, and concentrated. The residue was purifeid by flash column chromatography (silica gel; EtOAc/hexane = 1/1) to afford **22a** (239 mg, 68%) as a white amorphous substance. ^{1}H NMR (400 MHz, $CDCl_3$) δ 1.24−1.64 (m, 9H), 1.73−1.82 (m, 3H), 2.04−2.09 (m, 2H), 3.29 (td, *J* = 11.7, 2.0 Hz, 2H), 3.91 (dd, *J* = 11.4, 2.8 Hz, 2H), 4.04 (d, *J* = 7.1 Hz, 2H), 4.92−4.98 (m, 1H), 6.61 (s, 1H), 7.53 (d, *J* = 1.0 Hz, 1H), 7.70 (d, *J* = 1.0 Hz, 1H). MS-ESI (*m/z*) = 431 $[M+H]^+$.

***tert*-Butyl 6-(cyclohexyloxy)-3-iodoimidazo[1,2-*b*]pyridazin-8-yl((tetrahydro-2*H*-pyran-4-yl)methyl)carbamate (23a).** To a solution of **22a** (238 mg, 0.553 mmol) in DMF (5 mL) was added NIS (137 mg, 0.608 mmol). The reaction mixture was stirred at room temperature for 5 h and then diluted with EtOAc and water. The aqueous layer was separated and extracted with EtOAc. The combined organic extracts were washed with water and brine, dried over Na_2SO_4, filtered, and concentrated. The residue was purified by flash column chromatography (silica gel; EtOAc/hexane = 1/1) to afford **23a** (268 mg, 87%) as a white amorphous substance. ^{1}H NMR (400 MHz, CDCl3) δ 1.23−1.67 (m, 9H), 1.70−1.86 (m, 3H), 2.10−2.13 (m, 2H), 3.28 (td, *J* =

11.5, 1.7 Hz, 2H), 3.91 (dd, *J* = 11.4, 2.8 Hz, 2H), 4.00 (d, *J* = 7.1 Hz, 2H), 5.03−5.09 (m, 1H), 6.67 (s, 1H), 7.61 (s, 1H). MS-ESI (*m/z*) = 557 $[M+H]^+$.

4-(6-(Cyclohexyloxy)-8-((tetrahydro-2*H*-pyran-4-yl)methylamino)imidazo[1,2-*b*]pyridazin-3-yl)-*N*-cyclopropylbenzamide (24a). A mixture of **23a** (267 mg, 0.480 mmol), 4-(cyclopropylaminocarbonyl)phenylboronic acid pinacol ester (207 mg, 0.720 mmol), $PdCl_2$(dtbpf) (15.6 mg, 0.024 mmol), and K_2CO_3 (199 mg, 1.44 mmol) in DMF/H_2O (3 mL/0.3 mL) was heated at 50 °C for 2 h. The reaction mixture was allowed to cool to room temperature and then diluted with EtOAc and water. The aqueous layer was separated and extracted with EtOAc. The combined organic extracts were washed with water and brine, dried over Na_2SO_4, filtered, and concentrated. The residue was purified by flash column chromatography (silica gel; EtOAc/hexane = 4/1) to afford *tert*-butyl 6-(cyclohexyloxy)-3-(4-(cyclopropylcarbamoyl)phenyl)imidazo[1,2-*b*]pyridazin-8-yl((tetrahydro-2*H*-pyran-4-yl)methyl)carbamate (283 mg, 100%) as a white amorphous substance. MS-ESI (*m/z*) = 590 $[M+H]^+$. To a solution of this compound (283 mg) in DCM (3 mL) was added TFA (3 mL). The reaction mixture was stirred at room temperature for 30 min and then poured into aqueous K_2CO_3 solution. The mixture was extracted with EtOAc, and the combined organic extracts were then washed with water and brine, dried over Na_2SO_4, filtered, and concentrated. The residue was triturated with EtOAc, and the resulting solid was collected on a glass filter to afford **24a** (182 mg, 77%) as a white solid. ^{1}H NMR (400 MHz, $CDCl_3$) δ 0.62−0.68 (m, 2H), 0.90 (q, *J* = 6.3 Hz, 2H), 1.23−2.18 (m, 15H), 2.90−2.98 (m, 1H), 3.20 (t, *J* = 6.6 Hz, 2H), 3.40 (t, *J* = 11.2 Hz, 2H), 4.01 (dd, *J* = 3.5, 11.7 Hz, 2H), 4.90−4.99 (m, 1H), 5.65 (s, 1H), 5.72 (t, *J* = 6.1 Hz, 1H), 6.26 (s, 1H), 7.73 (s, 1H), 7.81 (d, *J* = 8.1 Hz, 2H), 8.16 (d, *J* = 8.1 Hz, 2H). MS-ESI (*m/z*) = 490 $[M+H]^+$.

***tert*-Butyl (tetrahydro-2*H*-pyran-4-yl)methyl(6-(1,1,1-trifluoro-2-methylpropan-2-ylamino)imidazo[1,2-*b*]pyridazin-8-yl)carbamate (25f).** A suspension of RuPhos (12.7 g, 27.3 mmol) and $Pd_2(dba)_3$ (6.24 g, 6.81 mmol) in dioxane (250 mL) was stirred at room temperature for 5 min. Sodium *t*-butoxide (21.0 g, 218 mmol), **18** (25 g, 68.1 mmol), and 1,1,1-trifluoro-2-methylpropan-2-amine hydrochloride (22.3 g, 136 mmol) was added to the suspension, and the reaction mixture was heated to reflux for 6 h. After cooling, the mixture was diluted with EtOAc and water. The aqueous layer was separated and extracted with EtOAc. The combined extracts were washed with water and brine, dried over $MgSO_4$, filtered, and concentrated. The residue was purified by flash column chromatography (silica gel, EtOAc/hexane, gradient: 30−100% EtOAc) to afford **25f** (22.1 g, 71%) as a tan solid. ^{1}H NMR (300 MHz, DMSO-d_6) δ 1.36 (s, 9H), 1.64 (s, 6H), 3.17 (t, J = 10.8 Hz, 2H), 3.74−3.83 (m, 4H), 6.74 (s, 1H), 6.90 (s, 1H), 7.39 (d, J = 1.1 Hz, 1H), 7.82 (d, J = 1.2 Hz, 1H). MS-ESI (*m/z*) = 458 $[M+H]^+$.

***tert*-Butyl 3-iodo-6-(1,1,1-trifluoro-2-methylpropan-2-ylamino)imidazo[1,2-*b*]pyridazin-8-yl((tetrahydro-2*H*-pyran-4-yl)methyl)carbamate (26f).** A mixture of **25f** (22.1 g, 48.3 mmol) and NIS (12.5g, 55.6 mmol) in DMF (200 mL) was stirred at room temperature for 14 h. The mixture was poured into aqueous $Na_2S_2O_3$ solution and then diluted with EtOAc. The aqueous layer was separated and extracted with EtOAc. The combined organic layer was washed with water and brine, dried over MgSO4, filtered, and concentrated to afford **25f** (26.9 g, 95%) as a tan solid. ^{1}H NMR (300 MHz, DMSO-d_6) δ 1.35 (s, 9H), 1.71 (s, 6H), 3.17 (t, J = 10.8 Hz, 2H), 3.75−3.78 (m, 4H), 6.80 (s, 1H), 7.10 (s, 1H), 7.51 (s, 1H). MS-ESI (*m/z*) = 584 $[M+H]^+$.

***N*-Cyclopropyl-4-(8-((tetrahydro-2*H*-pyran-4-yl)methylamino)-6-(1,1,1-trifluoro-2-methylpropan-2-ylamino)imidazo[1,2-*b*]pyridazin-3-yl)benzamide (27f).** A mixture of **26f** (26.9 g, 46.1 mmol), 4-(cyclopropylaminocarbonyl)phenylboronic acid pinacol ester (15.9 g, 55.3 mmol), $PdCl_2$(dtbpf) (3.77 g, 4.61 mmol), and aqueous Na_2CO_3 (2 M solution; 69.2 mL, 138

mmol) in DMF (250 mL) was heated at 50 °C for 4 h. The reaction mixture was allowed to cool to room temperature and then diluted with EtOAc and water. The insoluble materials were filtered off, and the aqueous layer was separated and extracted with EtOAc. The combined organic extracts were washed with water and brine, dried over $MgSO_4$, filtered, and concentrated. The residue was purified by flash column chromatography (silica gel; EtOAc/hexane, gradient: 20−70% EtOAc) to afford *tert*-butyl 3-(4-(cyclopropylcarbamoyl)phenyl)-6-(1,1,1-trifluoro-2-methylpropan-2-ylamino)imidazo[1,2-*b*]pyridazin-8-yl((tetrahydro-2*H*-pyran-4-yl)methyl)carbamate (26.8 g, 94%) as a brown solid. ^{1}H NMR (300 MHz, DMSO-d_6) δ 0.56−0.61 (m, 2H), 0.67-0.73 (m, 2H), 1.37 (s, 9H), 1.55 (d, J = 12.0 Hz, 2H), 1.66 (s, 6H), 1.98 (s, 2H), 2.81-2.90 (m, 1H), 3.19 (t, J = 10.8 Hz, 2H), 3.75−3.84 (m, 4H), 6.85 (s, 1H), 7.10 (s, 1H), 7.91 (d, J = 8.7 Hz, 2H), 7.96 (s, 1H), 8.12 (d, J = 8.7 Hz, 2H), 8.49 (d, J = 4.3 Hz, 1H). MS-ESI (*m/z*) = 617 $[M+H]^+$. To a solution of this compound (26.8 g) in DCM (90 mL) was added TFA (33.5 mL). The reaction mixture was stirred at room temperature for 15 h, diluted with $CHCl_3$ (300 mL), and then basified with aqueous $NaHCO_3$ solution. The aqueous layer was separated and extracted with $CHCl_3$. The combined organic extracts were washed with water, dried over $MgSO_4$, filtered, and concentrated. The residue was crystallized from methanol/ether to afford **27f** (17.5 g, 78%) as a tan solid. ^{1}H NMR (300 MHz, DMSO-d_6) δ 0.54−0.74 (m, 4H), 1.16−1.32 (m, 2H), 1.56-1.70 (m, 2H), 1.64 (s, 6H), 1.95 (m, 1H), 2.85 (m, 1H), 3.08 (t, J = 6.0 Hz, 2H), 3.22−3.34 (m, 2H), 3.81−3.92 (m, 2H), 5.80 (s, 1H), 6.47 (s, 1H), 7.11 (t, J = 6.0 Hz, 1H), 7.79 (s, 1H), 7.88 (d, J = 8.4 Hz, 2H), 8.15 (d, J = 8.4 Hz, 2H), 8.45 (d, J = 4.2 Hz, 1H). HRMS-ESI (*m/z*): $[M+H]^+$ calcd for $C_{26}H_{32}F_3N_6O_2$, 517.2533; found, 517.2535.

Biochemical Mps1 Assays. Mps1 kinase activity was measured by the DELFIA® (dissociation-enhanced lanthanide fluorescence immunoassay) method that monitors phosphorylation of the p38 MAPK peptide (biotin-AGAGLARHTDDEMTGYVA) using a

phosphorylated site specific antibody as described previously.[28] The protein preparation method for Mps1 was also reported in ref 28. Reported values are means of $n \geq 2$ determinations.

Cellular Mps1 Autophosphorylation Assays. Mps1 cellular activity was measured by detecting inhibition of autophosphorylation using RERF-LC-AI cells (RIKEN) that stably express FLAG-tagged Mps1 under the control of a tetracycline (Tet)-suppressible promoter. The detailed method was reported previously.[28] The reported values are means of $n = 2$ determinations. In all cases, individual measurements were within 2-fold for each compound.

Antiproliferative Assays. Antiproliferative activity was measured by the MTT (3-(4,5-di-methylthiazol-2-yl)-2,5-diphenyltetrazolium bromide) method using lung carcinoma cells A549 (ATCC), NCI-H460 (ATCC), Lu99 (RIKEN), and a normal cell MRC-5 (ATCC) as described previously.[28] The MRC-5 cells were seeded in a 96-well plate at 10000 cells/100 μL /well and incubated overnight. The reported values are means of $n \geq 2$ determinations. In all cases, individual measurements were within 2-fold for each compound. Antiproliferative assays using other cell lines were conducted at the National Cancer Center.[39]

Tumor Xenograft Models. NCI-H460 cells were cultured in the medium described in ref 28. NCI-H460 cells (1×10^6 to 1×10^7 cells) were inoculated subcutaneously into the flank of female nude mice (BALB/cA Jcl-nu/nu, 7 weeks old, CLEA Japan). The treatment was started when the tumor volumes reached around 200 mm^3. The test compound suspended in 0.5% methylcellulose solution (Wako) was administered po daily for 14 days ($n = 6$). Details have been described previously.[28] All mice had access to water and food ad libitum and all experiments were performed with the approval of the Shionogi Animal Care and Use Committee.

Solubility Assay. Japanese Pharmacopeia JP-2nd (JP-2) solution (pH 6.8) containing 20 mmol/L of sodium taurocholate was used as the aqueous buffer. The buffer was prepared as follows: JP-2 solution: phosphate buffer 500 mL and water 500 mL; JP-2 solution containing

sodium taurocholate: sodium taurocholate (1.08 g) and the JP-2 solution to reach 100 mL. For each compound, 0.2 mL of the JP-2 solution containing sodium taurocholate solution was added to 0.5 mg of dry compound, and the mixture was shaken for 1 h at 37 °C. The solution was filtered with a membrane filter (0.45 μm), and 0.1 mL of methanol was added to the filtrate (0.1 mL) so that the filtrate was diluted 2-fold. Quantification was performed by HPLC with an absolute calibration method.

Rat Microsomal Stability Studies. Rat microsomes were prepared from male Sprague-Dawley rats (8 weeks). The metabolic stability of test compounds in rat liver microsomes was determined at one concentration (0.1 μM). The compounds were incubated with 0.5 mg protein/mL in suspension in 50 mM Tris-HCl buffer (pH 7.4), 150 mM KCl, 10 mM $MgCl_2$, 1 mM β-NADPH at 37 °C. Microsomal incubations were initiated by the addition of 100-fold concentrated solution of the compounds. Incubations was terminated by addition of 2-fold volume of organic solvent (MeCN/MeOH = 1/1) after 0 and 30 minutes of incubation at 37 °C. The preparation protein was removed by centrifugation. The supernatants were analyzed by LC/MS/MS. All incubations were conducted in duplicate, and the percentage of compound remaining at the end of the incubation was determined from the LC/MS/MS peak area ratio.

Pharmacokinetic Studies. Male Sprague-Dawley rat (8 weeks) were purchased from Charles River Laboratories. Compounds were formulated as suspensions in 0.5% methylcellulose (0.2 mg/mL) and dosed orally at 1 mg/kg (n = 2) under the nonfasted condition. For iv study, the compounds were formulated as solutions in DMA/propylene glycol (1:1, 0.5 mg/mL) and dosed intravenously from the tail vein at 0.5 mg/kg (n = 2) under isoflurane anesthesia under the nonfasted condition. Details of the method has been described previously.[29] All experiments were performed with the approval of the Shionogi Animal Care and Use Committee.

Cocrystallization of Mps1 with 11f and 27b. Protein expression and purification were performed as described previously.[28] Cocrystals of Mps1 in complex with **11f** and **27b** were prepared using the sitting-drop vapor diffusion method. Equal volumes of protein solution (11.4 mg/mL containing 0.5 mM of **11f**, 6.8 mg/mL containing 0.5 mM of **27b**) and the mother liquor were mixed in a single droplet and equilibrated against 0.1 mL of mother liquor at 293 K. The mother liquor conditions were 0.1 M PIPES pH 6.5, 12.3% w/v PEG 5000, and 0.082 M magnesium sulfate for **11f** and 0.1 M Tris hydrochloride pH 7.5, 8.0% w/v triethylene glycol, and 0.12 M potassium chloride for **27b**. Data collection and structure solution were performed as described previously.[28]

Chart 1. Representative Potent Mps1 Inhibitors

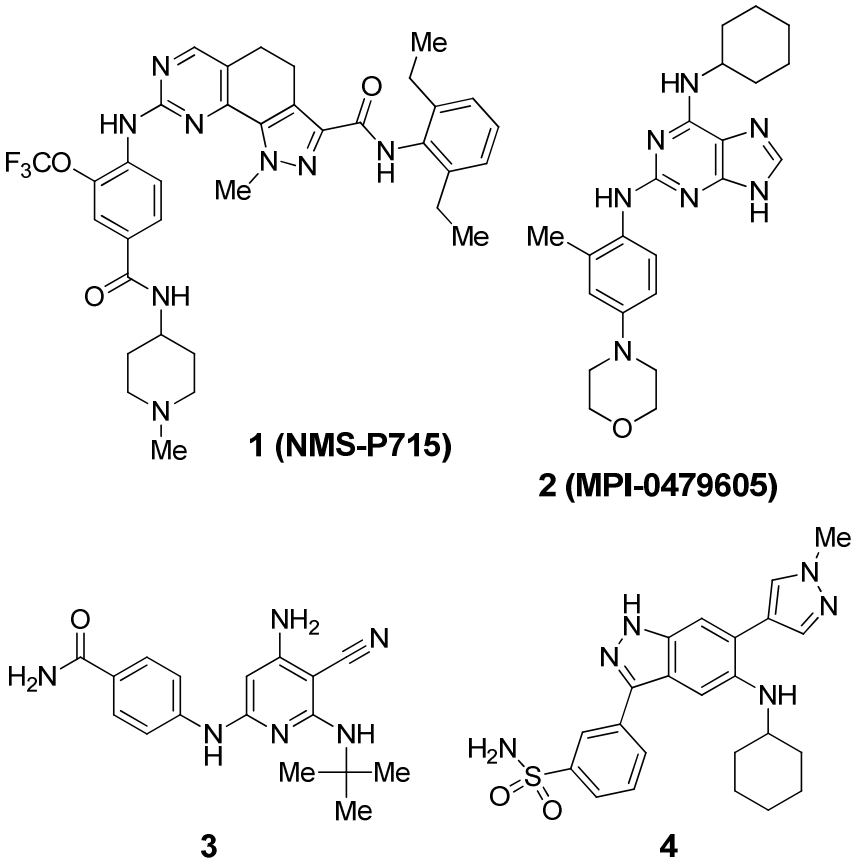

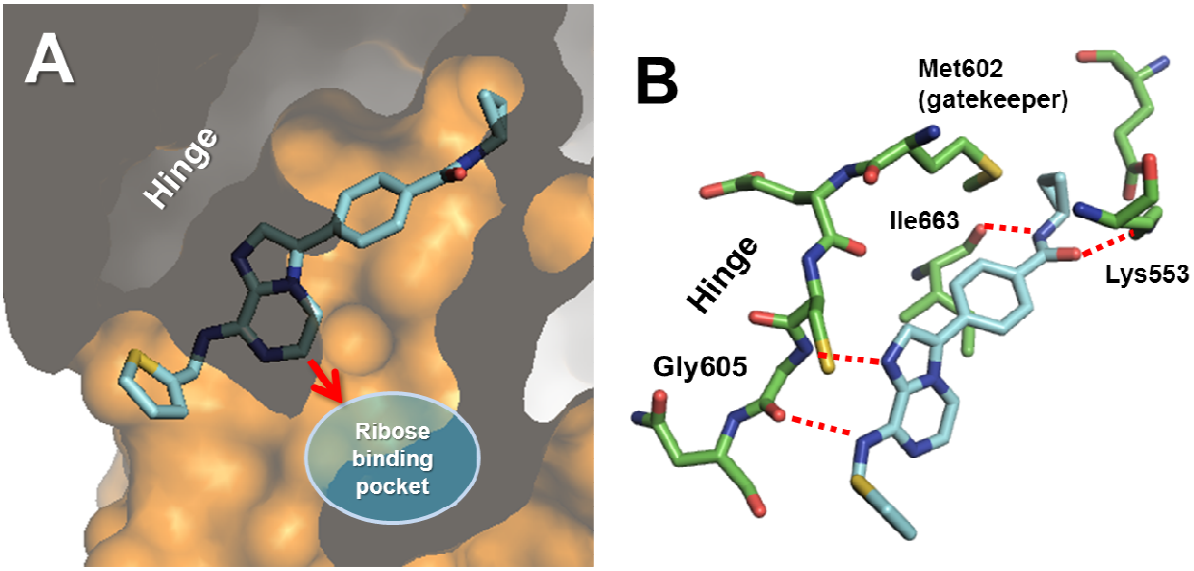

Figure 1. X-ray structure of **11f** bound to Mps1 (PDB ID: 3WZK). (A) Compound **11f** is shown as sticks with a cyan carbon. The pocket surface is orange. The ribose binding pocket is indicated in cyan. (B) Key residues are shown as sticks with green carbon. Hydrogen bonds are shown as dotted red lines. Figures were generated with PyMOL.[40]

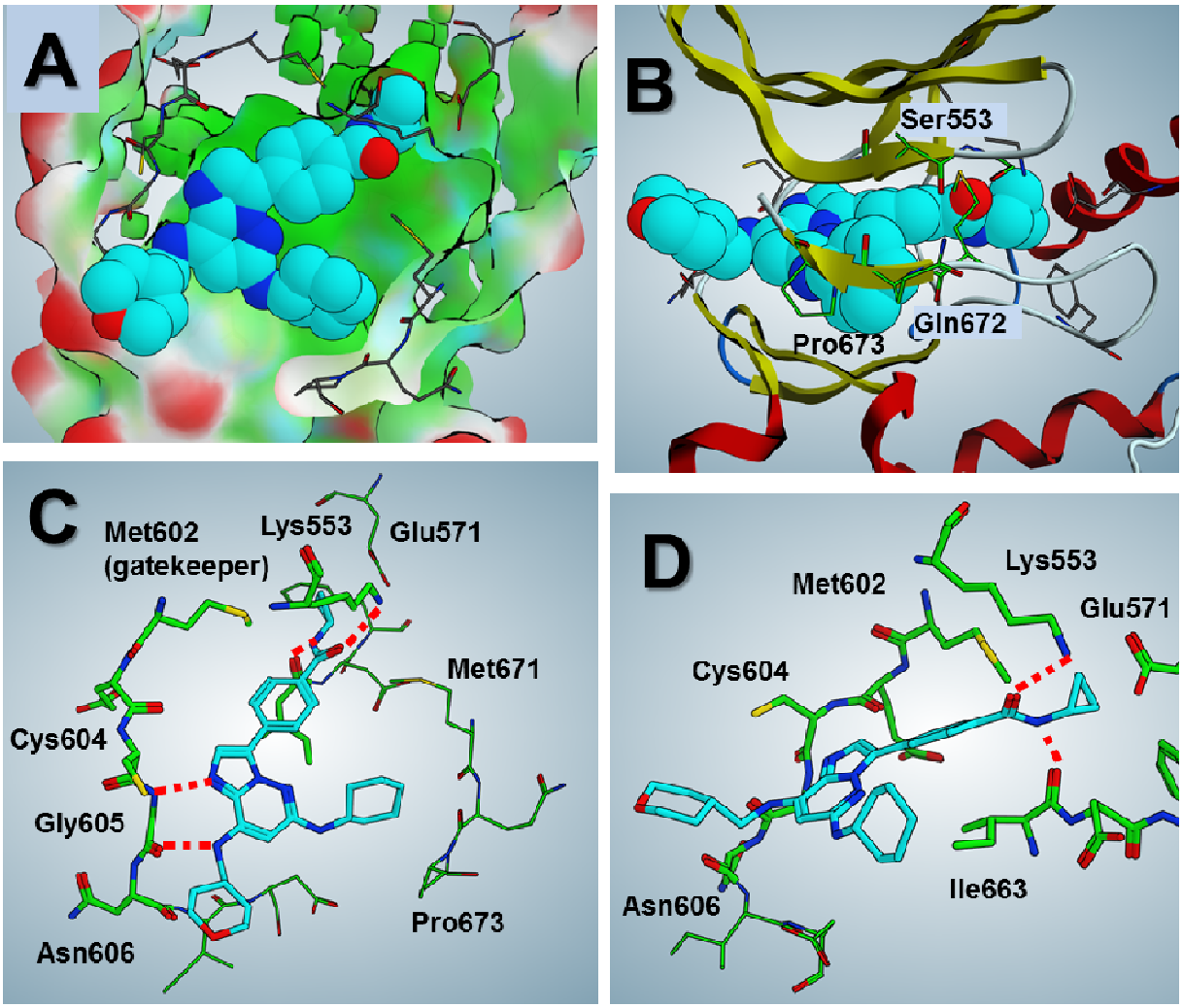

Figure 2. X-ray structure of **27b** bound to Mps1 (PDB ID: 3WZJ). (A) Compound **27b** is shown as CPK with cyan carbon. Key residues are shown as lines with gray carbon. Pocket surface is colored as follows: lipophilic, green; hydrophilic, cyan; solvent exposed, red. (B) Compound **27b** is shown as CPK with cyan carbon. Key residues are shown as sticks with green carbon. (C) Compound **27b** is shown as sticks with cyan carbon. Hydrogen bond interactions of **27b** with hinge region, Ile663, and Lys553 are shown as dotted red lines. Key residues are shown as sticks or lines with green carbon. (D) Hydrogen bond interactions of **27b** with Lys553 and Ile663 are shown as dotted red lines. Figures were generated with MOE (version 2013.08).[43]

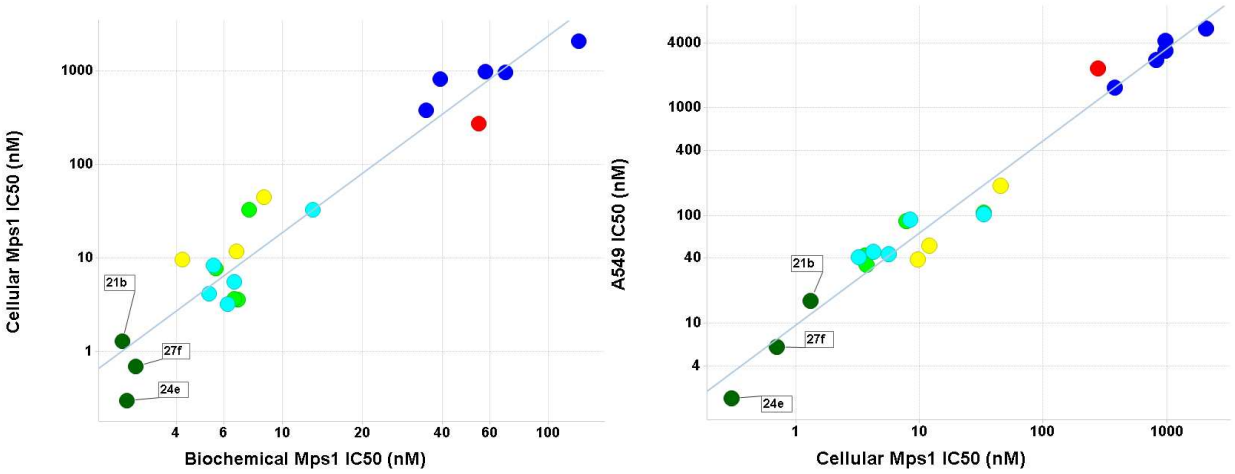

Figure 3. (A) Correlation between biochemical Mps1 IC_{50} and cellular Mps1 IC_{50} is shown. Logarithmic scale is used for both *x*- and *y*-axes. The compounds in Tables 1, 2, 3, 4, and 5 are colored red, blue, yellow, green, and cyan, respectively. Compounds **10b**, **10c**, **10d**, **10d**, and **11b** are not shown because cellular Mps1 IC_{50} values were not measured. Compounds **21b**, **24e**, and **27f** are highlighted in dark green. R^2 = 0.917. (B) Correlation between cellular Mps1 IC_{50} and A549 IC_{50} is shown. Other definitions are the same as Panel A, including the explanation of compounds not shown. R^2 = 0.969. The scatter plots were prepared using TIBCO Spotfire, version 4.5.0.

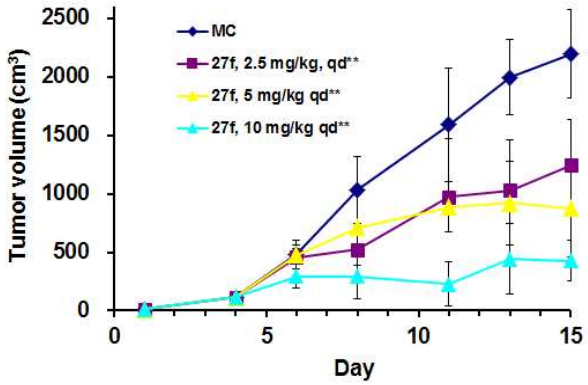

Figure 4. Effects of orally administered **27f** on the growth of NCI-H460 tumor. Asterisks indicate statistically significant differences from the vehicle-treated group based on Dunnett's *t* test (**$P \leq 0.01$). There was one death on day11 in the 5 mg/kg group and three deaths on day11 in the 10 mg/kg group.

Scheme 1. Synthesis of Imidazo[1,2-a]pyrazines 10a−d[a]

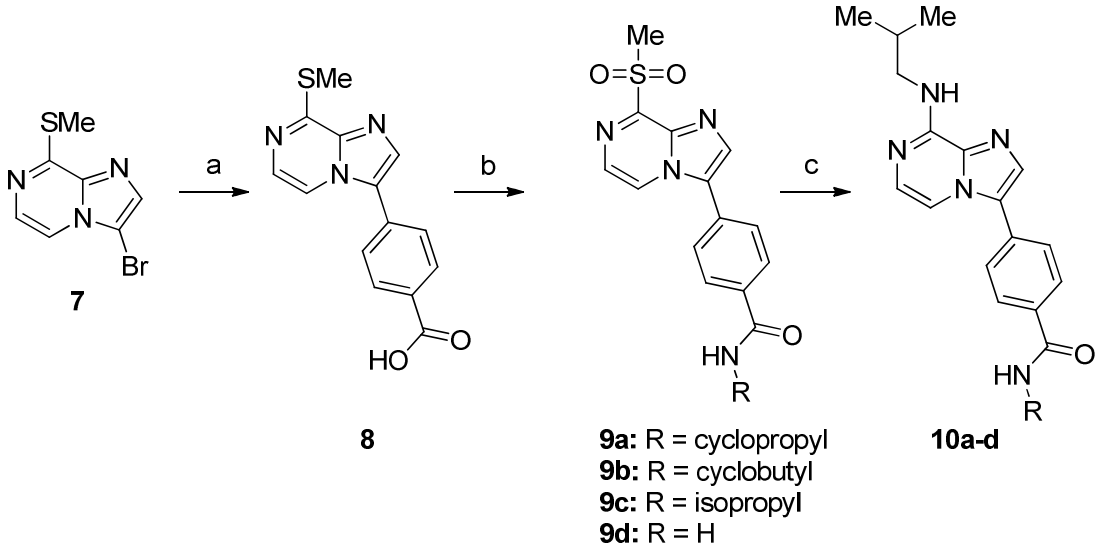

[a]Reagents and conditions: (a) (i) 4-methoxycarbonylphenylboronic acid pinacol ester, $PdCl_2(dppf)\cdot CH_2Cl_2$, aq. Na_2CO_3, dioxane, reflux; (ii) aq. LiOH, MeOH, 82%; (b) (i) HATU, DIEA, amine, DMF, rt; (ii) *m*-CPBA, $CHCl_3$, rt, 23−88%; (c) amine, dioxane, reflux, 14−95%.

Scheme 2. Synthesis of Imidazo[1,2-*a*]pyrazines 11a−f

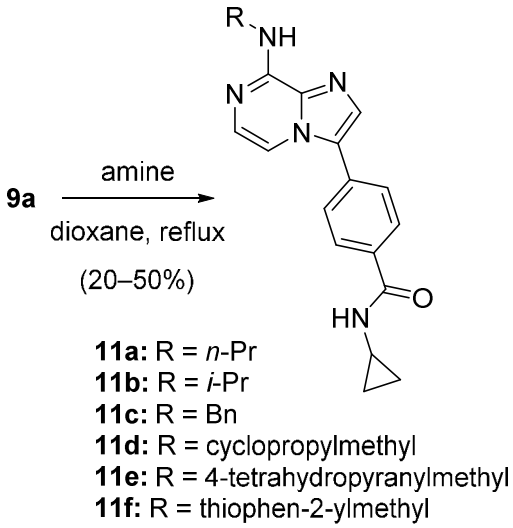

Scheme 2. Synthesis of Imidazo[1,2-*a*]pyrazines 15a−b[a]

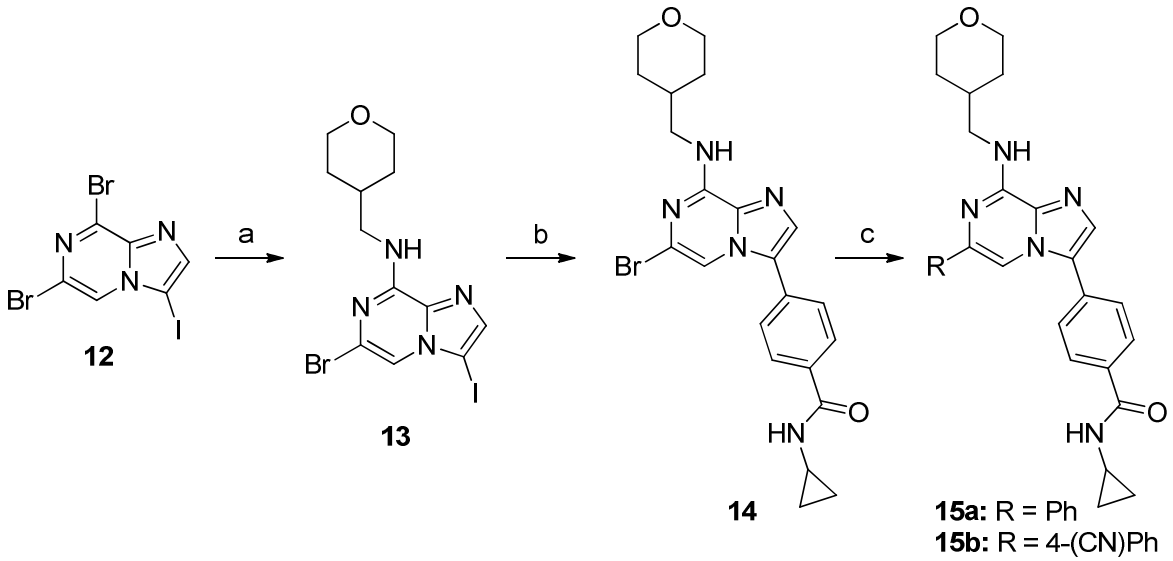

[a]Reagents and conditions: (a) 4-(aminomethyl)tetrahydropyran, DMA, 130 °C (microwave), 97%; (b) (4-(cyclopropylcarbamoyl)phenyl)boronic acid pinacol ester, $Pd(PPh_3)_4$, aq. Na_2CO_3, EtOH, 130 °C (microwave), 82%; (c) $PdCl_2(PPh_3)_2$, boronic acid, aq. Na_2CO_3, EtOH, 130 °C (microwave), 50−54%.

Scheme 4. Synthesis of 6-Arylimidazo[1,2-*b*]pyridazines 21a and 21b[a]

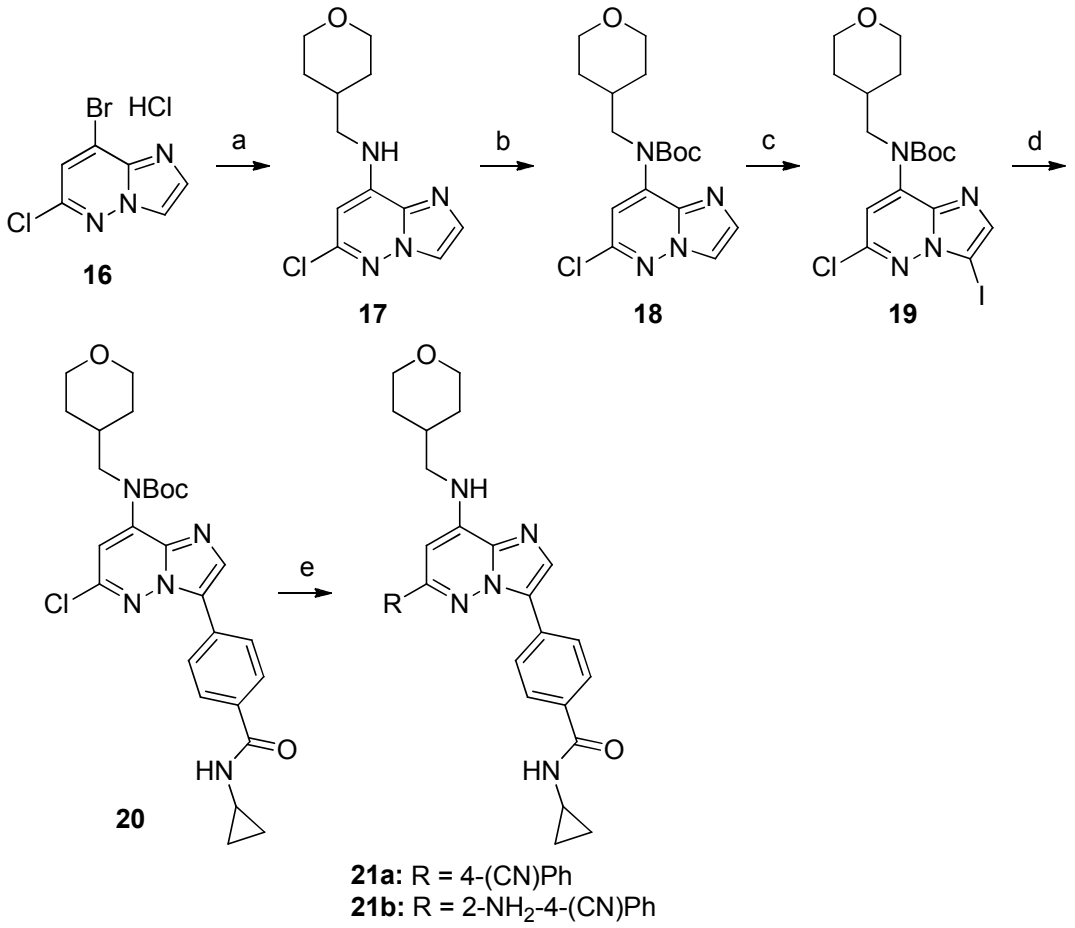

[a]Reagents and conditions: (a) (tetrahydro-2*H*-pyran-4-yl)methylamine, DIEA, EtOH, reflux, 71%; (b) Boc_2O, DMAP, THF, 50 °C, quant.; (c) NIS, DMF, 80 °C, 89%; (d) (4-(cyclopropylcarbamoyl)phenyl)boronic acid pinacol ester, $Pd(PPh_3)_4$, aq. Na_2CO_3, DMF, 100 °C, 55%; (e) (i) $RB(OH)_2$, $PdCl_2(dppf)\cdot CH_2Cl_2$, aq. Na_2CO_3, EtOH (ii) TFA, DCM, rt, 59%−quant.

Scheme 5. Synthesis of 6-Alkoxyimidazo[1,2-b]pyridazines 24a−e[a]

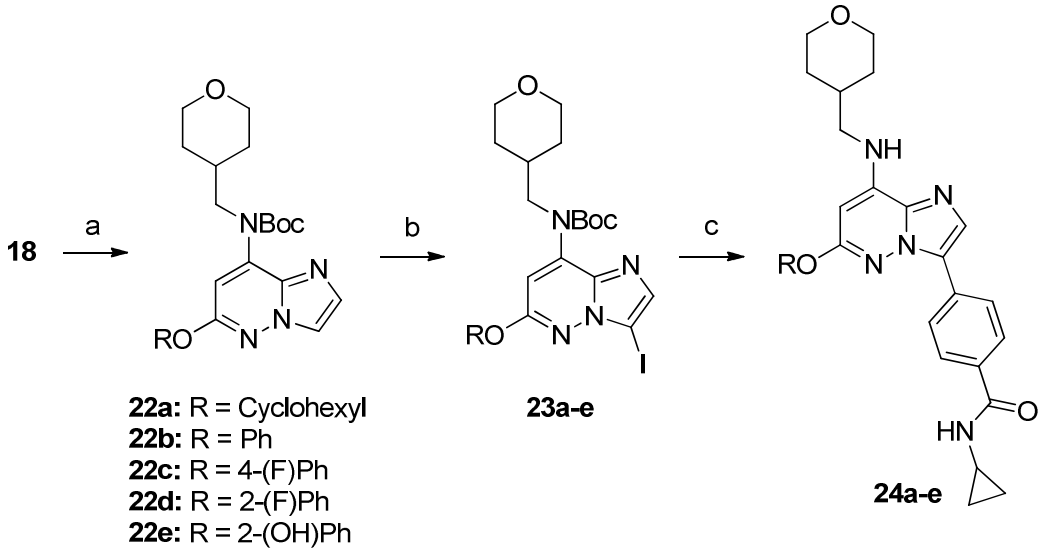

[a]Reagents and conditions: (a) ROH, NaH, NMP, rt, 51−68%; (b) NIS, DMF, rt, 84−94%; (c) (i) (4-(cyclopropylcarbamoyl)phenyl)boronic acid pinacol ester, $PdCl_2(dppf)\cdot CH_2Cl_2$, aq. Na_2CO_3, DMF, 50 °C; (ii) TFA, DCM, rt, 44−77%; **24e**: 20% over 3 steps.

Scheme 6. Synthesis of 6-Aminoimidazo[1,2-*b*]pyridazines 27a-f[a]

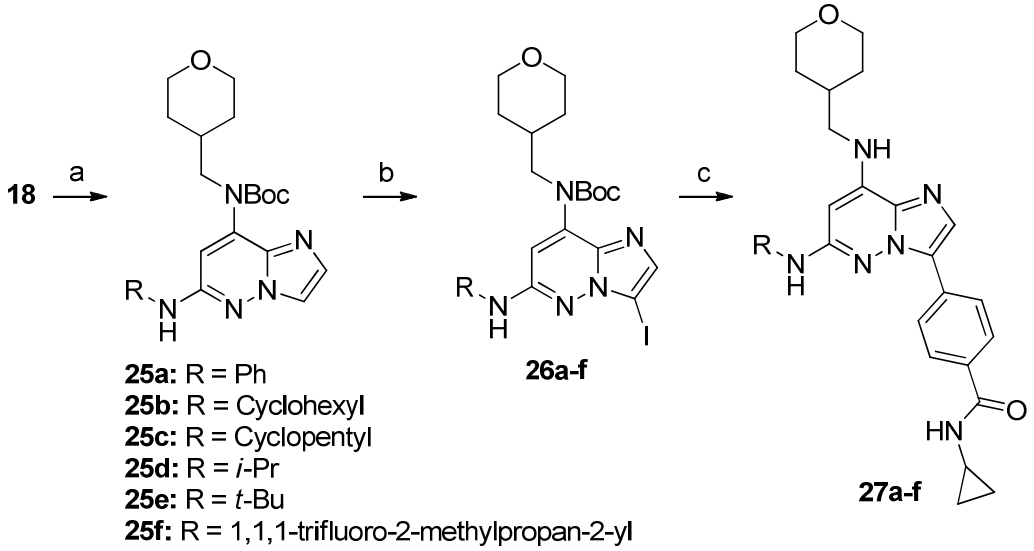

[a]Reagents and conditions: (a) RNH_2, $Pd(OAc)_2$, xantphos, K_2CO_3, dioxane, reflux, 62−80%; (b) NIS, DMF, rt, 85−100%; (c) (i) (4-(cyclopropylcarbamoyl)phenyl)boronic acid pinacol ester, $PdCl_2(dppf)\cdot CH_2Cl_2$, aq. Na_2CO_3, DMF, 50 °C; (ii) TFA, DCM, rt, 25−73%; **27a**: 41% over 3 steps.

Table 1. SAR of Amide Derivatives at the 3-Position[a]

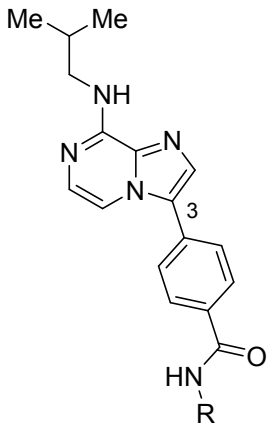

compd	R	Mps1 IC_{50} (nM)[b]
10a		55 ± 2.8[c]
10b	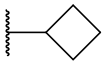	180 ± ND
10c		460 ± ND
10d	H	2500 ± ND

[a]Assay protocols are described in ref 28. [b]Biochemical assay. Average values of two determinations. ND = not determined. [c]An average value of three determinations with standard deviation.

Table 2. SAR of Amino Derivatives at the 8-Position[a]

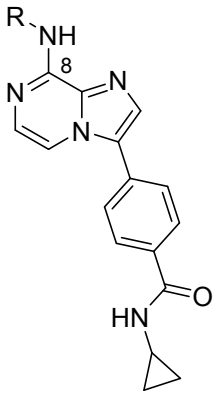

compd	R	Mps1 IC_{50} (nM)[b]
10a	*i*-Bu	55 ± 2.8
11a	*n*-Pr	69 ± 13
11b	*i*-Pr	490 ± ND[c]
11c	Bn	130 ± ND[c]
11d		39 ± 5.3
11e	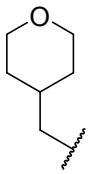	35 ± 1.4
11f	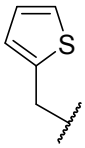	58 ± ND[c]

[a]Assay protocols are described in ref 28. [b]Biochemical assay. Average values of at least three determinations with standard deviation unless otherwise noted. [c]Average values of two determinations. ND = not determined.

Table 3. SAR of Aryl Derivatives at the 6-Position[a]

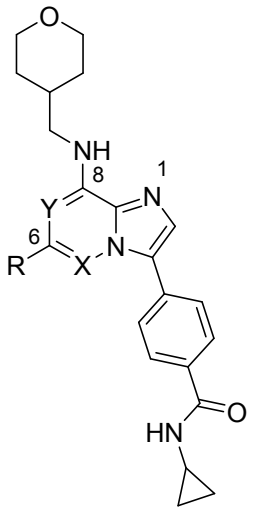

compd	X	Y	R	Mps1 IC_{50} (nM)[b]	Cellular IC_{50} (nM) pMps1[c]	Cellular IC_{50} (nM) A549[d]
11e	CH	N	H	35 ± 1.4	380	1500 ± 310
15a	CH	N	Ph	8.5 ± ND[e]	45	190 ± ND[e]
15b	CH	N	*p*-(CN)Ph	6.6 ± ND[e]	12	79 ± 19
21a	N	CH	*p*-(CN)Ph	4.2 ± 0.40	9.6	39 ± 4.7
21b	N	CH	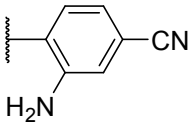	2.5 ± 0.10	1.3	16 ± 2.9

[a]Assay protocols are described in ref 28. [b]Biochemical assay. Average values of at least three determinations with standard deviation unless otherwise noted. [c]Inhibition of autophosphorylation in RERF cells. Average values of two determinations. [d]Cell viability in A549 cells after 72 h. Average values of at least three determinations with standard deviation unless otherwise noted. [e]Average values of two determinations. ND = not determined.

Table 4. SAR of Alkoxy Derivatives at the 6-Position[a]

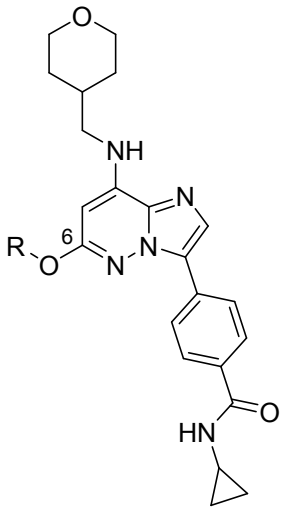

compd	R	Mps1 IC_{50} (nM)[b]	Cellular IC_{50} (nM) pMps1[c]	Cellular IC_{50} (nM) A549[d]
24a	Cyclohexyl	7.5	33	110 ± ND[e]
24b	Ph	6.8	3.6	42 ± ND[e]
24c	*p*-(F)Ph	5.6	7.8	88 ± ND[e]
24d	*o*-(F)Ph	6.6	3.7	35 ± 4.8
24e	*o*-(OH)Ph	2.6	0.30	2.0 ± 0.96

[a]Assay protocols are described in ref 28. [b]Biochemical assay. Average values of two determinations. [c]Inhibition of autophosphorylation in RERF cells. Average values of two determinations. [d]Cell viability in A549 cells after 72 h. Average values of at least three determinations with standard deviation unless otherwise noted. [e]Average values of two determinations. ND = not determined.

Table 5. SAR of Amino Derivatives at the 6-Position[a]

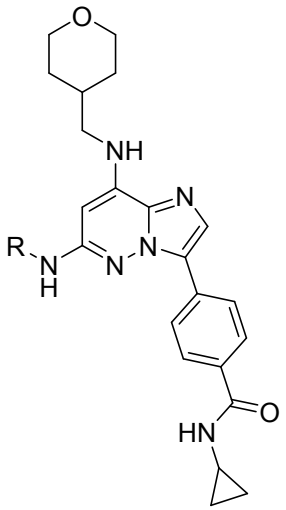

compd	R	Mps1 IC_{50} (nM)[b]	Cellular IC_{50} (nM) pMps1[c]	Cellular IC_{50} (nM) A549[d]
27a	Ph	13 ± ND[e]	33	300 ± ND[e]
27b	Cyclohexyl	6.6 ± 2.1	5.6	44 ± 2.8
27c	Cyclopentyl	5.3 ± 0.65	4.2	46 ± 15
27d	*i*-Pr	5.5 ± 1.0	8.4	91 ± 14
27e	*t*-Bu	6.2 ± 1.8	3.2	41 ± 2.1
27f	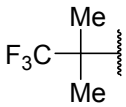	2.8 ± 0.22	0.70	6.0 ± 1.3

[a]Assay protocols are described in ref 28. [b]Biochemical assay. Average values of at least three determinations with standard deviation unless otherwise noted. [c]Inhibition of autophosphorylation in RERF cells. Average values of two determinations. [d]Cell viability in A549 cells after 72 h. Average values of at least three determinations with standard deviation unless otherwise noted. [e]Average values of two determinations. ND = not determined.

Table 6. Pharmacokinetic properties of compounds 24a, 24d, 27e and 27f in Sprague-Dawley Rat.

			iv (SD rat, 0.5 mg/kg, n = 2)		po (rat, 1 mg/kg, n = 2)		
Compd	Solubility (μg/ml)[a]	RLM (%)[b]	CL (ml/min/kg)[c]	V_{dss} (L/kg)[d]	AUC (ng·h/ml)[e]	C_{max} (ng/ml)[f]	F (%)[g]
15b	1.0	0	145	5.0	NC	0	0
21a	0.49	42	38	4.2	NC	0	0
21b	2.6	59	23	2.0	NC	0	0
24a	10	55	8.7	1.6	439	33	23
24d	8.0	39	22	2.0	126	16	16
24e	1.3	21	78	2.2	NC	0	0
27e	63	59	16	1.7	377	50	36
27f	29	41	11	1.3	360	38	24

[a] Thermodynamic solubility at pH 6.8 using the buffer containing 20 mmol/L of sodium taurocholate. [b]% remaining in rat liver microsome after 30 min. Average values of two determinations. [c] Plasma clearance. [d] Volume of distribution at steady state. [e] Plasma area under the curve. NC = not calculated. [f] Maximal plasma concentration. [g] Oral bioavailability.

Table 7. Antiproliferative Activities of 27f, Paclitaxel, MLN-8237 against Various Cancer Cell Lines

		IC_{50} (nM)[a]		
Origin	Cell line	**27f**	Paclitaxel	MLN-8237
Lung carcinoma	A549	6.0	13	230
	NCI-H460	10	10	NT[b]
	NCI-H358	320	7.9	100
	Lu99	4.7	5.2	62
	Lu116	6.1	5.1	97

	LC2/ad	17	2.5	77
	PC-14	9.8	4.4	170
Colon carcinoma	HCT15	6.3	240	740
	HCT116	9.4	6.1	95
	HT29	16	7.0	330
Pancrea carcinoma	MIA PaCa-2	8.1	6.1	130
Gastric carcinoma	GSS	5.3	3.4	39
Leukemia	MKN45	3.3	4.0	93
	HL60	9.1	7.9	74
Normal lung	MRC-5	>10000	80	>10000

[a]Cell viability after 72 h. [b]NT = Not tested.

Table 8. Pharmacokinetic Profile of Compound 27f in nu/nu Mouse[a]

	po (BALB/cAJcl-nu/nu mice, *n* =2)		
Dose[a]	C_{max} (ng/ml)[c]	AUC (ng·h/ml)[d]	T_{max} (h)
10	2426	8001	0.5
100	14028	48504	1.0

[a]Female BALB/cAJcl-nu/nu mice were dosed orally with a solution of 1 w/w%TPGS/0.5 w/w%PVP K90/5 w/w%EtOH/PEG400. [b]Maximal plasma concentration. [c]Plasma area under the curve. [d]Time to reach Cmax.

ASSOCIATED CONTENT

Kinase selectivity data for compounds **11e**, **24e**, and **27f** (Table S1), overlay of the co-crystal structures of **11f** and **27b** bound to Mps1 (Figure S1), body weight data in tumor xenograft study of **27f** (Figure S2), and spectral data for compounds **9b−d**, **10b−d**, **11a−f**, **15a**, **21b**, **22b−d**,

23b−d, **24b−e**, **25b−e**, **26b−e**, and **27a-e**. This material is available free of charge via the Internet at http://pubs.acs.org.

Accession Codes

PDB ID: 3WZK and 3WZJ (The crystal structures of **11f** and **27b** bound to Mps1, respectively)

AUTHOR INFORMATION

Corresponding Author

* Phone: +81 (6) 6331 6190. Fax: +81 (6) 6332 6385. E-mail: ken-ichi.kusakabe@shionogi.co.jp

Present Address

[∞]Department of Medicine, The University of Chicago, Chicago, Illinois 60637, United States.

Notes

The authors declare no competing financial interest.

ACKNOWLEDGMENTS

We thank Yoshio Hato, Jun Sato, Yusuke Tamura, Takuya Shintani, and Yasunori Mitsuoka for their support with the syntheses, and Naoko Umesako for her HRMS analysis. We gratefully thank Kenji Abe, Akira Kato, Norihiko Tanimoto, Takuji Nakatani, Hirosato Kondo, and Kohji Hanasaki for their helpful advice and suggestions during the course of this research. We are very grateful to Judy Noguchi for proofreading the manuscript.

ABBREVIATIONS

ABL_G250E, Abelson murine leukemia viral oncogene homolog 1 mutant (G250E); CAMK1, calcium/calmodulin-dependent protein kinase type 1; CIN, chromosomal instability; CLK2,

CDC-like kinase 2; DIEA, *N*,*N*-diisopropylethylamine; EtOAc, ethyl acetate; HATU, 1-[bis(dimethylamino)methylene]-1*H*-1,2,3-triazolo[4,5-*b*]pyridinium 3-oxid hexafluorophosphate; MeCN, acetonitrile; Mps1, monopolar spindle 1; NIS, *N*-iodosuccinimide; $PdCl_2$(dppf) DCM, [1,1'-bis(diphenylphosphino)ferrocene]dichloropalladium(II) complex with dichloromethane; $PdCl_2$(dtbpf), [1,1'-bis(di-*tert*-butylphosphino)ferrocene]dichloropalladium(II); RLM, rat liver microsomes; RuPhos, 2-dicyclohexylphosphino-2',6'-diisopropoxybiphenyl; SD, Sprague-Dawley; TTK, TTK protein kinase.

REFERENCES

(1) Nowell, P. C. The clonal evolution of tumor cell populations. *Science* **1976**, *194*, 23−28

(2) Lengauer, C.; Kinzler, K. W.; Vogelstein, B. Genetic instabilities in human cancers. *Nature* **1998**, *396*, 643−649.

(3) Negrini, S.; Gorgoulis, V. G.; Halazonetis, T. D. Genomic instability - an evolving hallmark of cancer. *Nat. Rev. Mol. Cell Biol.* **2010**, *11*, 220−228.

(4) Duesberg, P.; Rausch, C.; Rasnick, D.; Hehlmann, R. Genetic instability of cancer cells is proportional to their degree of aneuploidy. *Proc. Natl. Acad. Sci. U.S.A.* **1998**, *95*, 13692−13697.

(5) Daniel, J.; Coulter, J.; Woo, J.-H.; Wilsbach, K.; Gabrielson, E. High levels of the Mps1 checkpoint protein are protective of aneuploidy in breast cancer cells. *Proc. Natl. Acad. Sci. U.S.A.* **2011**, *108*, 5384−5389.

(6) Mills, G. B.; Schmandt, R.; McGill, M.; Amendola, A.; Hill, M.; Jacobs, K.; May, C.; Rodricks, A. M.; Campbell, S.; Hogg, D. Expression of TTK, a novel human protein kinase, is associated with cell proliferation. *J. Biol. Chem.* **1992**, *267*, 16000−16006.

(7) Lauze, E.; Stoelcker, B.; Luca, F. C.; Weiss, E.; Schutz, A. R.; Winey, M. Yeast spindle pole body duplication gene MPS1 encodes an essential dual specificity protein kinase. *EMBO J.* **1995**, *14*, 1655−1663.

(8) Abrieu, A.; Magnaghi-Jaulin, L.; Kahana, J. A.; Peter, M.; Castro, A.; Vigneron, S.; Lorca, T.; Cleveland, D. W.; Labbe, J.-C. Mps1 is a kinetochore-associated kinase essential for the vertebrate mitotic checkpoint. *Cell* **2001**, *106*, 83−93.

(9) Stucke, V. M.; Sillje, H. H. W.; Arnaud, L.; Nigg, E. A. Human Mps1 kinase is required for the spindle assembly checkpoint but not for centrosome duplication. *EMBO J.* **2002**, *21*, 1723−1732.

(10) Fisk, H. A.; Mattison, C. P.; Winey, M. Human Mps1 protein kinase is required for centrosome duplication and normal mitotic progression. *Proc. Natl. Acad. Sci. U.S.A.* **2003**, *100*, 14875−14880.

(11) Abrieu, A.; Magnaghi-Jaulin, L.; Kahana, J. A.; Peter, M.; Castro, A.; Vigneron, S.; Lorca, T.; Cleveland, D. W.; Labbe, J.-C. Mps1 is a kinetochore-associated kinase essential for the vertebrate mitotic checkpoint. *Cell* **2001**, *106*, 83−93.

(12) Saito-Hisaminato, A.; Katagiri, T.; Kakiuchi, S.; Nakamura, T.; Tsunoda, T.; Nakamura, Y. Genome-wide profiling of gene expression in 29 normal human tissues with a cDNA microarray. *DNA Res.* **2002**, *9*, 35−45.

(13) Kikuchi, T.; Daigo, Y.; Katagiri, T.; Tsunoda, T.; Okada, K.; Kakiuchi, S.; Zembutsu, H.; Furukawa, Y.; Kawamura, M.; Kobayashi, K.; Imai, K.; Nakamura, Y. Expression profiles of

non-small cell lung cancers on cDNA microarrays: Identification of genes for prediction of lymph-node metastasis and sensitivity to anti-cancer drugs. *Oncogene* **2003**, *22*, 2192−2205.

(14) Yamabuki, T.; Daigo, Y.; Kato, T.; Hayama, S.; Tsunoda, T.; Miyamoto, M.; Ito, T.; Fujita, M.; Hosokawa, M.; Kondo, S.; Nakamura, Y. Genome-wide gene expression profile analysis of esophageal squamous cell carcinomas. *Int. J. Oncol.* **2006**, *28*, 1375−1384.

(15) Yuan, B.; Xu, Y.; Woo, J.-H.; Wang, Y.; Bae, Y. K.; Yoon, D.-S.; Wersto, R. P.; Tully, E.; Wilsbach, K.; Gabrielson, E. Increased expression of mitotic checkpoint genes in breast cancer cells with chromosomal instability. *Clin. Cancer Res.* **2006**, *12*, 405−410.

(16) Schmidt, M.; Budirahardja, Y.; Klompmaker, R.; Medema, R. H. Ablation of the spindle assembly checkpoint by a compound targeting Mps1. *EMBO Rep.* **2005**, *6*, 866−872.

(17) Hewitt, L.; Tighe, A.; Santaguida, S.; White, A. M.; Jones, C. D.; Musacchio, A.; Green, S.; Taylor, S. S. Sustained Mps1 activity is required in mitosis to recruit O-Mad2 to the Mad1-C-Mad2 core complex. *J. Cell Biol.* **2010**, *190*, 25−34.

(18) Kwiatkowski, N.; Jelluma, N.; Filippakopoulos, P.; Soundararajan, M.; Manak, M. S.; Kwon, M.; Choi, H. G.; Sim, T.; Deveraux, Q. L.; Rottmann, S.; Pellman, D.; Shah, J. V.; Kops, G. J. P. L.; Knapp, S.; Gray, N. S. Small-molecule kinase inhibitors provide insight into Mps1 cell cycle function. *Nat. Chem. Biol.* **2010**, *6*, 359−368.

(19) Langdon, S. R.; Westwood, I M.; van Montfort, R. L. M.; Brown, N.; Blagg, J. Scaffold-Focused Virtual Screening: Prospective Application to the Discovery of TTK Inhibitors *J. Chem. Inf. Model.* **2013**, *53*, 1100−1112.

(20) Santaguida, S.; Tighe, A.; D'Alise, A. M.; Taylor, S. S.; Musacchio, A. Dissecting the role of MPS1 in chromosome biorientation and the spindle checkpoint through the small molecule inhibitor reversine. *J. Cell Biol.* **2010**, *190*, 73−87.

(21) Naud, S.; Westwood, I. M.; Faisal, A.; Sheldrake, P.; Bavetsias, V.; Atrash, B.; Cheung, K.-M. J.; Liu, M.; Hayes, A.; Schmitt, J.; Wood, A.; Choi, V.; Boxall, K.; Mak, G.; Gurden, M.; Valenti, M.; de Haven Brandon, A.; Henley, A.; Baker, R.; McAndrew, C.; Matijssen, B.; Burke, R.; Hoelder, S.; Eccles, S. A.; Raynaud, F. I.; Linardopoulos, S.; van Montfort, R. L. M.; Blagg, J. Structure-based design of orally bioavailable 1*H*-pyrrolo[3,2-*c*]pyridine inhibitors of mitotic kinase monopolar spindle 1 (MPS1). *J. Med. Chem.* **2013**, *56*, 10045−10065.

(22) Lan, W.; Cleveland, D. W. A chemical tool box defines mitotic and interphase roles for Mps1 kinase. *Cell Biol.* **2010**, *190*, 21–24.

(23) Colombo, R.; Caldarelli, M.; Mennecozzi, M.; Giorgini, M. L.; Sola, F.; Cappella, P.; Perrera, C.; Depaolini, S. R.; Rusconi, L.; Cucchi, U.; Avanzi, N.; Bertrand, J. A.; Bossi, R. T.; Pesenti, E.; Galvani, A.; Isacchi, A.; Colotta, F.; Donati, D.; Moll, J. Targeting the mitotic checkpoint for cancer therapy with NMS-P715, an inhibitor of MPS1 kinase. *Cancer Res.* **2010**, *70*, 10255–10264.

(24) Caldarelli, M.; Angiolini, M.; Disingrini, T.; Donati, D.; Guanci, M.; Nuvoloni, S.; Posteri, H.; Quartieri, F.; Silvagni, M.; Colombo, R. Synthesis and SAR of new pyrazolo[4,3-h]quinazoline-3-carboxamide derivatives as potent and selective MPS1 kinase inhibitors. *Bioorg. Med. Chem. Lett.* **2011**, *21*, 4507–4511.

(25) Tardif, K. D.; Rogers, A.; Cassiano, J.; Roth, B. L.; Cimbora, D. M.; McKinnon, R.; Peterson, A.; Douce, T. B.; Robinson, R.; Dorweiler, I.; Davis, T.; Hess, M. A.; Ostanin, K.;

Papac, D. I.; Baichwal, V.; McAlexander, I.; Willardsen, J. A.; Saunders, M.; Christophe, H.; Kumar, D. V.; Wettstein, D. A.; Carlson, R. O.; Williams, B. L. Characterization of the cellular and antitumor effects of MPI-0479605, a small-molecule inhibitor of the mitotic kinase Mps1. *Mol. Cancer Ther.* **2011**, *10*, 2267–2275.

(26) Vijay K., D.; Hoarau, C.; Bursavich, M.; Slattum, P.; Gerrish, D.; Yager, K.; Saunders, M.; Shenderovich, M.; Roth, B. L.; McKinnon, R.; Chan, A.; Cimbora, D. M.; Bradford, C.; Reeves, L.; Patton, S.; Papac, D. I.; Williams, B. L.; Carlson, R. O. Lead optimization of purine based orally bioavailable Mps1 (TTK) inhibitors. *Bioorg. Med. Chem. Lett.* **2012**, *22*, 4377–4385.

(27) Colombo, R.; M. Caldarelli, M.; Giorgini, M. L.; Milani, O.; Avanzi, N.; Sola, F.; Pesenti, E.; Donati, D; Galvani, A.; In *NMS-P153, a tight-binder inhibitor of the spindle assembly checkpoint kinase MPS1*, Proceedings of 24th EORTC-NCI-AACR Symposium on Molecular Targets and Cancer Therapeutics, Dublin, Ireland, Nov 6-9, 2012; Abstract #517.

(28) Kusakabe, K.; Ide, N.; Daigo, Y.; Itoh, T.; Higashino, K.; Okano, Y.; Tadano, G.; Tachibana, Y.; Sato, Y.; Inoue, M.; Wada, T.; Iguchi, M.; Kanazawa, T.; Ishioka, Y.; Dohi, K.; Tagashira, S.; Kido, Y.; Sakamoto, S.; Yasuo, K.; Maeda, M.; Yamamoto, T.; Higaki, M.; Endoh, T.; Ueda, K.; Shiota, T.; Murai, H.; Nakamura, Y. Diaminopyridine-based potent and selective Mps1 kinase inhibitors binding to an unusual flipped-peptide conformation. *ACS Med. Chem. Lett.* **2012**, *3*, 560−564.

(29) Kusakabe, K.; Ide, N.; Daigo, Y.; Tachibana, Y.; Itoh, T.; Yamamoto, T.; Hashizume, H.; Hato, Y.; Higashino, K.; Okano, Y.; Sato, Y.; Inoue, M.; Iguchi, M.; Kanazawa, T.; Ishioka, Y.; Dohi, K.; Kido, Y.; Sakamoto, S.; Yasuo, K.; Maeda, M.; Higaki, M.; Ueda, K.; Yoshizawa, H.; Baba, Y.; Shiota, T.; Murai, H.; Nakamura, Y. Indazolebased potent and cell-active Mps1 kinase

inhibitors: Rational design from pan-kinase inhibitor anthrapyrazolone (SP600125). *J. Med. Chem.* **2013**, *56*, 4343−4356.

(30) Bennett B. L.; Sasaki D. T.; Murray B. W.; O'Leary E. C.; Sakata S. T.; Xu W.; Leisten J. C.; Motiwala A.; Pierce S.; Satoh Y.; Bhagwat S. S.; Manning A. M.; Anderson D. W. SP600125, an anthrapyrazolone inhibitor of Jun N-terminal kinase. *Proc. Natl. Acad. Sci. U.S.A.* **2001**, *98*, 13681−13686.

(31) Compound **10a** was purchased from BioFocus DPI Limited. http://www.biofocus.com/ (accessed May 6, 2013)

(32) In parallel with our research, Bayer group reported imidazo[1,2-*a*]pyrazine and imidazo[1,2-*b*]pyridazine scaffolds as Mps1 inhibitors: (a) Koppitz, M.; Klar, U.; Jautelat, R.; Kosemund, D.; Bohlmann, R.; Bader, B.; Lienau, P.; Siemeister, G. Preparation of imidazopyrazines for use as Mps-1 and TKK inhibitors in the treatment hyperproliferative disorders. PCT Int. Appl. WO 2012080229 A1 20120621, 2012. (b) Klar, U.; Koppitz, M.; Jautelat, R.; Kosemund, D.; Bohlmann, R.; Lienau, P.; Siemeister, G.; Wengner, A. M. Preparation of substituted imidazopyridazines as monopolar spindle 1 kinase inhibitors for treating hyperproliferative and angiogenesis disorders. PCT Int. Appl. WO 2012032031 A1 20120315, 2012. (c) Jemaa, M.; Galluzzi, L.; Kepp, O.; Senovilla, L.; Brands, M.; Boemer, U.; Koppitz, M.; Lienau, P.; Prechtl, S.; Schulze, V.; Siemeister, G.; Wengner, A. M.; Mumberg, D.; Ziegelbauer, K.; Abrieu, A.; Castedo, M.; Vitale, I.; Kroemer, G. Characterization of novel MPS1 inhibitors with preclinical anticancer activity. *Cell Death Differ.* **2013**, *20*, 1532−1545.

(33) Kusakabe, K.; Yoshida, H.; Nozu, K.; Hashizume, H.; Tadano, G.; Sato, J.; Tamura, Y.; Mitsuoka, Y. Preparation of fused imidazole derivatives having TTK kinase inhibitory activity.

PCT Int. Appl. WO 2011013729 A1 20110203, 2011. (U.S. Pat. Appl. Publ. US 20120059162 A1 20120308, 2012).

(34) Guzi, Timothy J.; Paruch, Kamil; Dwyer, Michael P.; Zhao, Lianyun; Curran, Patrick J.; Belanger, David B.; Hamann, Blake; Reddy, Panduranga A.; Siddiqui, M. Arshad. Preparation of novel imidazopyrazines as cyclin dependent kinase inhibitors. U.S. Pat. Appl. Publ. US 20060106023 A1 20060518, 2006.

(35) Vaccaro, W.; Chen, Z.; Dodd, D. S.; Huynh, T. N.; Lin, J.; Liu, C.; Mussari, C. P.; Tokarski, J. S.; Tortolani, D. R.; Wrobleski, S. T. Preparation of fused heterocyclic compounds useful as kinase modulators. PCT Int. Appl. WO 2007038314 A2 20070405, 2007.

(36) ChemBioDraw Ultra, version 13.0.2.3021; PerkinElmer: Cambridge, MA, 2013.

(37) Wani, Mansukhlal C.; Taylor, Harold Lawrence; Wall, Monroe E.; Coggon, Philip; McPhail, Andrew T. Plant antitumor agents. VI. Isolation and structure of taxol, a novel antileukemic and antitumor agent from Taxus brevifolia. *J. Am Chem. Soc.* **1971**, *93*, 2325−2327.

(38) Gorgun Gullu; Calabrese Elisabetta; Hideshima Teru; Ecsedy Jeffrey; Perrone Giulia; Mani Mala; Ikeda Hiroshi; Bianchi Giada; Hu Yiguo; Cirstea Diana; Loredana, S.; Yu-Tzu, T.; Sabikun, N.; Mei, Z.; Madhavi, B.; Ruben D. C.; Noopur, R.; Nikhil, M.; Paul, R.; Kenneth C. A. A novel Aurora-A kinase inhibitor MLN8237 induces cytotoxicity and cell-cycle arrest in multiple myeloma. *Blood* **2010**, *115*, 5202−5213.

(39) National Cancer Center. http://www.ncc.go.jp/en/ (accessed May 6, 2013)

(40) PyMOL, version 0.98; DeLano Scientific: San Carlos, CA.

(41) Janssen, Aniek; Kops, Geert J. P. L.; Medema, Rene H. Elevating the frequency of chromosome mis-segregation as a strategy to kill tumor cells. *Proc. Natl. Acad. Sci. U.S.A.* **2009**, *106*, 19108−19113.

(42) Laufer, R.; Ng, G.; Liu, Y.; Patel, N. K. B.; Edwards, L. G.; Lang, Y.; Li, S.-W.; Feher, M.; Awrey, D. E.; Leung, G.; Beletskaya, I.; Plotnikova, O.; Mason, J. M.; Hodgson, R.; Wei, X.; Mao, G.; Luo, X.; Huang, P.; Green, E.; Kiarash, R.; Lin, D. C.-C.; Harris-Brandts, M.; Ban, F.; Nadeem, V.; Mak, T. W.; Pan, G. J.; Qiu, W.; Chirgadze, N. Y.; Pauls, H. W. Discovery of inhibitors of the mitotic kinase TTK based on N-(3-(3-sulfamoylphenyl)-1H-indazol-5-yl) acetamides and carboxamides. *Bioorg. Med. Chem.* **2014**, *22*, 4968−4997.

(43) MOE, version 2013.08; Chemical Computing Group: Montreal, Canada, 2005.

Table of Contents graphic.

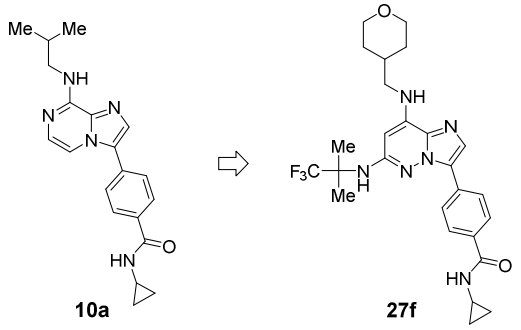

10a
Mps1 IC_{50} = 55 nM
Cellular Mps1 IC_{50} = 276 nM
A549 IC_{50} = 1112 nM

27f
Mps1 IC_{50} = 2.8 nM
Cellular Mps1 IC_{50} = 0.70 nM
A549 IC_{50} = 6.0 nM